

FINAL REPORT FOR MSC PROJECT

DEPARTMENT OF BIOENGINEERING

Printed Stretchable Sensors

Author:

Daniel Elabd

Supervisors:

Panagiotis Kassanos

Etienne Burdet

Submitted in partial fulfilment of the requirements for the award of MSc in
Biomedical Engineering from Imperial College London

September 17, 2020

Word count: 5980

Abstract

Stretchable sensors are becoming increasingly popular in a variety of fields, which use inks based on elastomers with conductive fillers. This paper aims to characterise the conductive-inks and the printing processs to demonstrate a strain gauge sensor using graphite-PDMS. The strain sensor was fabricated and demonstrates a gauge factor of approximately 10.49. This sensor realisation is a step towards realising a more complex multiparameter sensing system (including ECG, temperature etc) which can be implemented in wearables and soft robotics.

Acknowledgments

I would like to express my gratitude to my supervisor Dr Panagiotis Kassanos for his guidance, support and motivation throughout the entirety of the project. I would also like to thank Professor Etienne Burdet for giving me the opportunity to work with the Human Robotics group. I would like to express my gratitude to Minghao Hu, Dr Meysam Keshavarz and Dr Mohamed Abdelaziz for their help and advice. Finally, a special thank you to my family and friends for their constant support throughout this period.

Contents

1	Introduction	1
1.1	Developed stretchable sensors	1
1.1.1	Sensors for physiological monitoring	1
1.1.2	Strain gauge, pressure and force sensors	1
1.1.3	3D printing of sensors	2
1.2	Aims and Objectives	3
1.3	Theoretical Background	4
1.3.1	PDMS	4
1.3.2	Elastomeric-conductive composites: an insulator-conductor transition	4
1.3.3	Piezoresistivity of PDMS composites	4
1.3.4	Strain gauges	5
2	Materials and Methods	6
2.1	Ink Fabrication and Optimisation	6
2.1.1	Fabrication process	6
2.1.2	Conductive filler concentration	7
2.1.3	Viscosity optimisation	7
2.2	PDMS Substrate Fabrication	8
2.3	Extruding Nozzles/Needles	8
2.4	Print Files	9
2.5	Printer and Print Parameters Optimisation	9
2.5.1	Characterisation	10
2.6	Design and Fabrication of the Sensor	11
2.6.1	Wires and pads	11
2.6.2	Material configurations and printing	12
2.7	Experimental Procedure	13
2.7.1	Preparation	13
2.7.2	Testing procedure for stretching	13
2.7.3	Testing procedure for bending	14
3	Results	15
3.1	Characterisation of Printed Lines	15
3.2	Characterisation of Sensors	15
3.2.1	Stretching	15
3.2.2	Bending	16
4	Discussion	21
4.1	Characterisation of Printed Lines	21
4.1.1	Track width versus pressure	21
4.1.2	Track width versus speed	21
4.2	Characterisation of the Sensor	21
4.2.1	Stretching	21

4.2.2 Bending	22
5 Conclusion	23
5.1 Future Work	23
5.1.1 Further testing for all-graphite sensor	23
5.1.2 Testing for all-silver and graphite-silver hybrid sensors	23
5.1.3 Develop a fully stretchable multiparameter sensing system	23
5.1.4 Embedded printing in uncured PDMS	23
5.2 Summary	23
References	25
A G-Code Scripts	29
A.1 All-graphite-PDMS G-code script	29
A.2 All-silver-PDMS G-code script	35
A.3 Graphite- & silver-PDMS hybrid G-code script	44

1 Introduction

There is increased demand for flexible and stretchable electronics across a wide range of technologies, enabling state-of-the-art electronics to perform while being stretched, bent or deformed. Applications include stretchable displays [1, 2], sensing skin for soft robotics [3, 4], wearable circuits/devices [5, 6] and stretchable sensors for physiological monitoring [7–10]. Due to the growing need for continuous patient monitoring, there is increased focus on stretchable sensors in order to prioritise patient comfort in daily life. Soft robotics is also a rapidly growing field which has high demand for stretchable sensors that allow for feedback control, essentially acting as an electronic skin.

1.1 Developed stretchable sensors

There are many cutting edge approaches towards fabricating stretchable alternatives to the common rigid sensors available. Various approaches are presented and discussed in the following paragraphs.

1.1.1 Sensors for physiological monitoring

Chuang and Wereley have developed a stretchable microheater and temperature sensor [11]. The conductive ink they used consists of silver-coated copper flakes. The sensor demonstrated heating capability and a good temperature sensing range (with limitations). Another approach by Shih et al. [7] found that graphite, compared to other carbon fillers, is the most sensitive to temperature variation. They present the use of a graphite-PDMS composite in fabricating a temperature sensor array which was successful in continuously monitoring variations in temperature.

Electrochemical sensing is another field where stretchable sensors are highly desired. An electrochemical sensor which records glucose levels and other parameters is presented by Bandodkar et al. [12]. Carbon nanotubes (CNTs) and Ag/AgCl-Ecoflex inks are used with an Ecoflex substrate as opposed to PDMS. The same team previously attempted an electrochemical device using poly(3,4-ethylenedioxythiophene)-poly(styrenesulfonate) (PEDOT:PSS) [13] which is a conducting polymer. However, it provides limited stretchability when compared to their more recent approach [12]. Another stretchable glucose and pH sensor is presented by Oh et al. [14]. This included the use of Au nanosheets and CNTs, with a PDMS substrate. Using sweat, it successfully detects the glucose and pH levels while undergoing stretching or deformation.

1.1.2 Strain gauge, pressure and force sensors

An increasingly popular application of stretchable sensors is pressure/force sensing. These sensors have uses such as monitoring human motion and acting as a sensing skin for soft robotics. Abshirini et al. present a strain gauge sensor based on CNTs-PDMS [15]. The sensitivity of strain gauges is determined by the gauge factor, this is

discussed more thoroughly in section 1.3. The gauge factor of this sensor was found to be 4.3. A conventional (metallic) strain gauge has a gauge factor of 2.0 [16]. The sensor was used to detect the bending motion of a human wrist. Another strain gauge sensor was developed by Lu et al. using both CB-PDMS (for sensing element) and CNT-PDMS (for interconnects) [17] which demonstrated a gauge factor of 29. The reason for this higher value is due to the material used; CB-PDMS has a higher resistivity and is more strain-dependent [17] whilst CNT-PDMS exhibits the opposite and is therefore used for interconnects. This sensor was implemented in a similar manner to the former. Muth et al. present a wearable glove with strain sensors for each finger [18], enabling the motion detection of individual fingers. The materials used were conductive carbon grease (carbon black particles suspended in silicone oil) and Ecoflex. The gauge factor computed from the sensors was 3.8.

There is a plethora of different strain gauges fabricated from a variety of different materials, including graphene-PDMS [19], silver nanocomposites-PDMS [20] and others [21]. A review published by Amjadi et al. [22] compares different material strain gauges and their performance in terms of gauge factor and stretchability.

Pressure sensors have been developed for soft robotics, such as the soft prosthetic hand in [3]. CB-PDMS on a PDMS substrate is used and demonstrates grasping tasks with the sensors. Cheng et al. also present a robotic e-skin using a tactile sensing array [23] which successfully recorded external applied pressure. The sensing element was fabricated from carbon black, silver and copper nano-powders introduced into PDMS.

From the literature, we observe many different types of sensors with a wide range of materials for fabricating them. The choice of material depends on various factors, mainly the specific sensor application. Other factors include the cost and availability. For example, we observe that most strain gauge and pressure sensors use carbon-based materials such as carbon black or graphite. For interconnects and integration with electrical components (ICs, SMDs) silver-based inks are used such as in [24] and [25], since silver has a higher conductivity than carbon. We also observed that electrochemical sensing is more complex, where more intricate hybrid materials are used. McCoul et al. present a review [26] which compares the mechanical, electrical as well as other properties of different conducting polymers and hybrid materials used for stretchable sensors.

1.1.3 3D printing of sensors

There are many methods used in fabricating stretchable sensors. These mainly include stencil printing, screen printing, inkjet printing and finally extrusion based/3D printing. Stencil and screen printing are labour-intensive and time consuming. They require a mask and contact for sensor fabrication. Stencil printing also does not allow the printing of closed patterns, such as a circle. Inkjet printing solves these issues but is cannot print with high viscosity inks [27]. This paper reviews printing techniques and includes a table showing ink viscosity and minimum feature size for

different methods of printing. The solution to these limitations is therefore extrusion based printing, which can print using high viscous inks, requires no contact, automates and speeds up the process. It also enables easier fabrication of 3D structures when compared with other methods.

Reference	Material & sensor application	Extruding nozzle inner diameter (μm)	Minimum track width (μm)
[28]	Graphene-PDMS strain insensitive temperature sensor	250	310
[29]	PDMS+PTFE in a Triboelectric Nanogenerator	610	—
[30]	Graphene-PDMS tunable strain sensor	210	340
[31]	Ag Flakes-TPU capacitive sensor	510	200-400

Table 1: Comparison of print parameters and feature sizes for extrusion-based printing of stretchable sensors

The table shows some 3D printing approaches for different sensors, with the extruding nozzle diameter and minimum track width shown. In the literature, we see that the resolution/minimum track width was not a main consideration.

1.2 Aims and Objectives

The literature shows that there are different fabrication processes such as stencil or screen printing which have limitations. The use of additive techniques such as extrusion-based printing allows for low-cost, low-waste (use of direct writing rather than throwing away excess from stencils/molds), automated processes that do not require a clean lab.

Previous work has been done to fabricate and optimise graphite-PDMS and Ag-PDMS conductive inks (by Hu et al. [32]), where stencil printing and molding techniques have been used to fabricate sensors. This project aims to assess the use of these inks with extrusion-based printing as an alternative technique, and to examine how different fabrication techniques can be used for the realisation of different types of sensors. It is also a step towards assessing the use of a hybrid fabrication process in developing stretchable sensors.

Therefore, the objectives of this project are as follows: to use custom-fabricated elastomer-conductive filler inks (graphite- or silver-PDMS), optimising them for 3D printing. The printing parameters/process would also be optimised through a characterisation process using an Allevi 2 Bioprinter. One objective through this optimisation is to reach (as much as possible) the commercial PCB resolution which consists of 100 μm for both track width and separation. The optimisation would also then be

used to print stretchable sensors for physiological monitoring and/or soft robotics. This would then be an initial step towards fabricating a single multiparameter system that incorporates sensors for bioimpedance, ECG, EMG, temperature, chemicals, force as well as heaters.

1.3 Theoretical Background

1.3.1 PDMS

Polydimethylsiloxane (PDMS, empirical formula $(C_2H_6OSi)_n$) is a silicon-based organic polymer, or elastomer, that is commercially available. It is a physically and chemically stable silicone rubber [33]. Because of its attractive physical and chemical attributes (compared to other elastomers), it is widely used in the stretchable sensors field. These include high flexibility, low curing temperature, high compressibility, non-toxicity, bio-compatibility and other properties [33].

1.3.2 Elastomeric-conductive composites: an insulator-conductor transition

Polymers are usually electrically insulating, however, by adding conductive particles into the polymer matrix (such as graphite or silver), conductive paths are formed [34]. These paths arise from two different mechanisms: mechanical contact between the conductive particles and electron tunnelling; a quantum-mechanical effect where under certain conditions, electrical current can flow through insulator materials [35].

To achieve conductivity, the percolation threshold must be reached. This is the minimum amount of conductive particles (usually expressed as a wt%) introduced into the polymer matrix that will give rise to the mentioned conductivity mechanisms. The percolation threshold will vary depending on the conductive filler used, where the material conductivity increases with filler concentration. However, high concentrations can cause the composite to become stiff and easy to break which defeats the purpose of using an elastomer. Therefore, there is a trade-off between conductivity and stretchability.

Many papers have captured the variation of mechanical and electrical properties against both filler type and concentration [25, 32, 36]. Examples include graphite, silver and several different types of carbon black. Research by Hu et al. [32] presents a comparison between three types of carbon black and graphite. Depending on the specific device and application, a suitable filler type and concentration is chosen.

1.3.3 Piezoresistivity of PDMS composites

A piezoresistive material experiences a reversible change in electrical resistance with applied strain. PMDS conductive composites possess this attribute due to percolation theory. Conductive particles in the polymer matrix create percolation networks, and the size of these networks determines the conductivity of the material. When strain is applied, such as stretching, the networks are disturbed and the distance between

particles increases (hence smaller networks). This results in a decreased probability of possessing the conductivity mechanisms previously mentioned. Therefore, the electrical resistance of the material increases. When the applied strain is removed, the resistance is restored to its original value after a specific amount of time due to its hysteresis nature.

1.3.4 Strain gauges

Strain gauge sensors are used in a wide range of technologies such as force sensing. For a standard, metallic strain gauge, when strain is applied, the resistance changes (similar behaviour to the piezoresistive effect). However, here the principle of the resistance variation lies in the geometry; when the conductor is stretched, its length increases (hence the cross section decreases) which induces an increase in resistance.

Strain sensors made of stretchable conductive composites are increasingly popular as they have higher sensitivity than their rigid counterparts. This is because of the combination of the geometry-based resistance variation with the piezoresistivity effect mentioned earlier [37]. For any strain gauge sensor, the sensitivity is expressed by the gauge factor k , which is defined as the ratio of the normalised change in resistance to the applied strain. This is expressed in equation 1:

$$k = \frac{\Delta R/R_0}{\Delta L/L_0} \quad (1)$$

where R_0 is the unstrained resistance of the sensor and the denominator is the strain (ε) defined as the ratio of elongation or change in length, ΔL , to the original length, L_0 .

2 Materials and Methods

To optimise the printing process, there were five main processes to configure. These include the ink fabrication and optimisation, the PDMS substrate fabrication, the extruding needles, the print files and the print parameters. After configuration, a sensor design was realised and set up for testing. In this section, each of these elements will be thoroughly discussed.

2.1 Ink Fabrication and Optimisation

2.1.1 Fabrication process

The fabrication process of the graphite conductive ink used is presented in figure 1. Firstly, the desired amount of PDMS (Sylgard 184, Dow Corning, USA) was poured and heptane (Sigma-Aldrich, product no. 246654) was added at a ratio of PDMS:heptane = 1:0.5. The purpose of the heptane is to allow for homogeneous mixing and viscosity control. This was mixed using a mixer (LH Overhead Stirrer, Velp Scientifica, Italy) at 1,400 rpm for 2 minutes. The solution was then placed in an ultrasonication bath (FB15049, Fisherbrand, Fischer Scientific, USA) for 2 minutes. The same process was repeated for graphite but with a heptane ratio of graphite:heptane = 1:0.25. (Sigma-Aldrich, product no. 282863, < 20 μm) in a separate container. Both solutions were then added together and mixed for 4 minutes at 1400 rpm. Finally, the curing agent was added (curing agent:PDMS = 1:10) and the mixture was mixed for a further 2 minutes to give the final graphite-PDMS conductive ink to be used in printing.

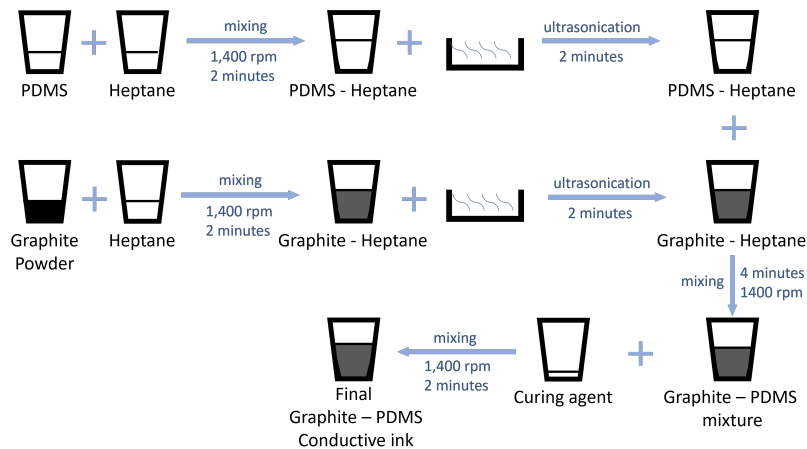


Figure 1: Graphite ink fabrication process

Due to the heavier nature of silver particles, a more rigorous fabrication technique is needed in order to suspend the silver particles within the PDMS matrix, this is shown in figure 2. The PDMS-heptane was fabricated as previously. The silver particles were weighed and heptane was added until the silver particles were completely

submerged. The mixture was mixed at 1400 rpm for one minute, then placed in the ultrasonication bath for another minute. This was repeated three times. The PDMS-heptane mixture is then added to the Ag-heptane and is mixed for 2 minutes, then ultrasonicated for a further 2 minutes. Again, this process was repeated three times. The curing agent was then added at the same ratio and the ink was mixed for 10 minutes. At this point the ink is submerged in heptane and the silver particles deposit. The ink is placed in the oven at 70 °C until all the heptane has evaporated, leaving behind the final Ag-PDMS ink.

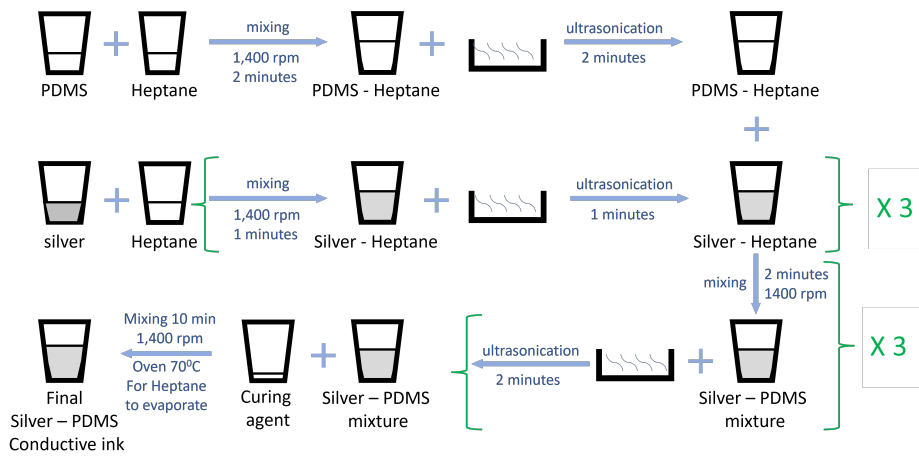


Figure 2: Silver ink fabrication process

2.1.2 Conductive filler concentration

The concentration of the conductive filler determines the conductivity of the final ink. The cited paper [32] shows how the conductivity varies as a function of graphite concentration. Based on this, a conductivity of 45 wt% was used for graphite which will yield a conductivity of approximately 62 S m^{-1} . This concentration of graphite was used as it provides a suitable balance between high conductivity and stretchability. For silver the same reasoning applies, where a concentration of 70 wt% was used. This value is quoted from private communications with Minghao Hu (lead of the previously cited paper [32]) from unpublished data for silver concentrations.

2.1.3 Viscosity optimisation

As previously mentioned, viscosity control is achieved using heptane. The amount of heptane added was optimised based on several factors, mainly the extruding needle profile and diameter (discussed thoroughly in section 2.3). For the purposes of this project, it was found that suitable viscosities were achieved with the ratios of heptane stated in the fabrication processes. Through a trial and error process, a higher viscosity resulted in frequent needle clogging whilst a lower viscosity resulted in a large ink spread. The viscosity was empirically optimised based on these ratios and not measured due to limited laboratory equipment. However, the same protocol was

consistently followed when fabricating inks. Further investigation will need proper instrumentation to measure and characterise viscosity.

2.2 PDMS Substrate Fabrication

Pure PDMS samples were fabricated as substrates for printing geometries/sensors. Figure 3 illustrates the fabrication process. Petri dishes of size 90 mm in diameter were used. These were first cleaned with IPA (isopropyl alcohol) and then soap water was poured in each. The soap water is then removed and the Petri dishes were placed on a hotplate at 130 °C for around ten minutes to dry. The purpose of this step is that it allows the easy and effective removal of the PDMS substrate from the Petri dish, as the dry soap residue acts as a release agent.

PDMS was poured in a cup (2 g per Petri dish) and heptane was added (twice the amount of PDMS poured). A large amount of heptane is required so that the liquid is of a very low viscosity to ensure the flatness of the PDMS substrate. The curing agent was also added at a ratio of curing agent : PDMS = 1:10 and the mixture was mixed for four minutes. The total weight of the mixture was then equally divided amongst the number of Petri dishes, where they were degassed using a desiccator for ten minutes. Finally, the samples were placed in the oven and cured for two hours at 70 °C.

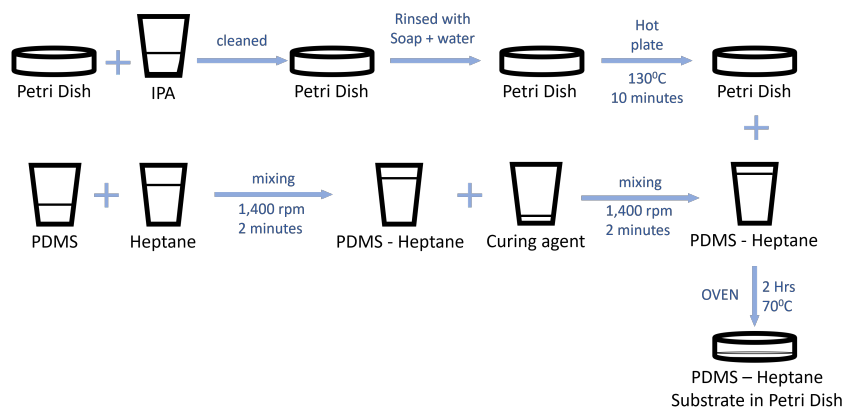


Figure 3: PDMS substrate fabrication process

2.3 Extruding Nozzles/Needles

There are two important parameters regarding the extruding needle; the needle profile and diameter. There are two types of profiles as illustrated in figure 4. Tapered needles require less extruding pressure and shear stress. They are also less prone to clogging than straight ones, as the material is pushed through a smaller distance. These reasons enabled finer printing, hence the tapered profile was used throughout the printing process.

As for the needle diameter, a higher gauge (i.e. a smaller inner diameter) will lead to a finer resolution. The diameter however is limited by the size of the conductive filler particles. For graphite-PDMS ink, the smallest diameter possible was 27 AWG (0.20 mm) as the size of graphite particles was $< 20 \mu\text{m}$. A smaller nozzle size would result in clogging. For Ag-PDMS, silver particles were of size 2–3 μm , allowing for extrusion with 32 AWG needles (0.10 mm).

Other parameters such as needle material and length are not considered as the conductive ink used is unaffected by the material. The length is more relevant when using straight needles and embedded/FRESH printing methods such as in [38].



Figure 4: Extruding nozzle profiles

2.4 Print Files

The next process to be configured is the type of print files being used. There are several file formats that can be used in 3D printing, examples being STL or OBJ files rendered from CAD software. 'Slicing' software converts these CAD drawings into strings of code known as G-code. This programming language defines all parameters of the print process such as the print speed, extruding pressure and direction and sequence of printing, which are usually automatically determined by the slicing software. By writing custom G-code scripts, designs can be defined with precise control over the mentioned parameters. For example, a design can be defined where each part of the design can be printed at a different desired speed or pressure. In the case of this project and several others, the sequence of printing different sections of a design, as well as the direction of printing (e.g. printing a line from top to bottom), is vital to ensure a high quality realisation. The use of STL files does not allow for this type of control, therefore custom written G-code scripts were written. The scripts used for this project are included in appendix A.

2.5 Printer and Print Parameters Optimisation

The printer model used is an Allevi 2 3D Bioprinter, which is a dual pneumatic extrusion-based system (shown in figure 5). It is controlled via the company's online



Figure 5: The Allevi 2 3D Bioprinter

software solution Allevi Bioprint Online.

The print parameters include the extruding pressure, print speed and layer height (the height at which the nozzle prints away from the substrate). These require optimisation to ensure high quality prints. For the layer height, Allevi's online guides recommend starting with the needle diameter. However, this was found to be too close to the substrate as the ink does not have enough space to escape, resulting in missing sections. The layer height was increased to around $80\ \mu\text{m}$ for both graphite- and Ag-PDMS inks. A larger layer height would result in rough geometrical features (e.g. edges and corners).

2.5.1 Characterisation

The print speed and pressure were optimised via a characterisation process. Figure 6 shows a design on a Petri dish with four identical groups of lines where the line separation is gradually decreasing. To characterise the effect of both pressure and speed, two different tests were performed. The first test, shown in figure 6a, involves printing each of the four groups at different pressures for a fixed speed. Figure 6b shows an example of the second test (vice versa) where each group is printed at a different speed for a fixed pressure.

The two tests were repeated for a wider range of pressures (2.0–7.5 psi for graphite-PDMS, 4.0–9.5 psi for Ag-PDMS at increments of 0.5 psi) and speeds (10–20 mms^{-1} for both inks at increments of 2 mms^{-1}). The designs were printed on Petri dishes and cured in the oven at $70\ ^\circ\text{C}$ for two hours, and the track width and separation were measured under a microscope (Keyence VHX-2000). For each group, the track width was measured for three lines where each was measured three times along its length. The average values were computed and the variation of track width versus pressure/speed was captured, this is presented in section 3.1. This characterisation process resulted in the optimisation of the extruding pressure and the print speed.

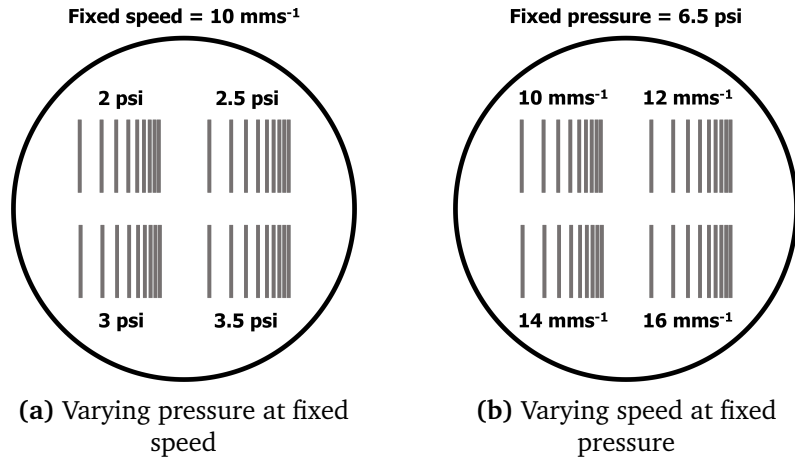


Figure 6: Characterisation tests for optimising extruding pressure and print speed

2.6 Design and Fabrication of the Sensor

Following the optimisation of the print parameters, a strain gauge sensor was designed using G-code scripts. It is always easiest to examine a strain gauge sensor first as the sensor is simple to fabricate. Therefore, for demonstration of stretchable sensors a strain gauge was designed.

Figure 7 shows the sensor design and geometry. There are two parts to the design; the strain sensing element itself and the wires and pads for testing purposes. Regarding the sensing element, there is no need for a meander-like/serpentine pattern like that associated with metallic strain gauges because the material being used is already piezoresistive. A simple design was realised to demonstrate the printer resolution together with a strain gauge sensor.

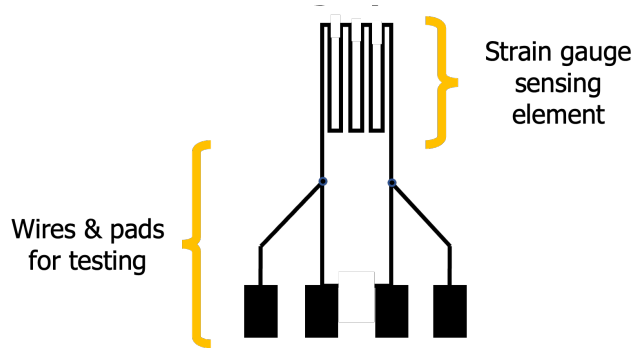


Figure 7: Strain gauge sensor design

2.6.1 Wires and pads

Two small circular blobs were printed at the intersections between the wires and the sensor to ensure proper connections. Four pads are required as this allows us to measure the four-point resistance of only the sensing element and not the entire

geometry. Current is forced through the two outer pads and the voltage is measured across the inner two pads (hence across the sensing element) which is then used to calculate the resistance of the sensor. This is discussed in more detail in section 2.7

2.6.2 Material configurations and printing

Different G-code scripts (see appendix A) were used to define three material configurations of the same design; all-graphite, all-silver and graphite-silver hybrid, shown in figure 8.

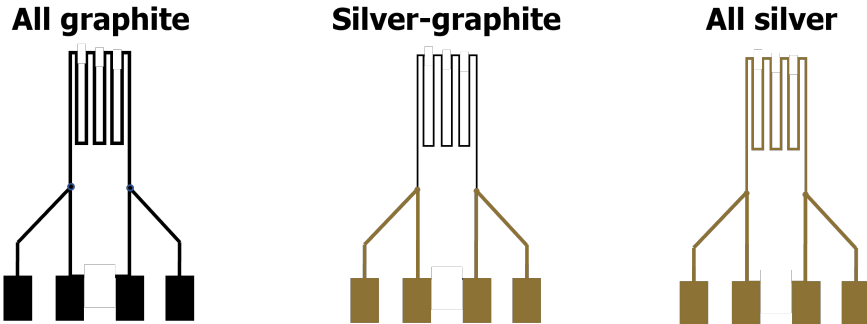


Figure 8: Different material configurations of the strain gauge sensor

The all-graphite and all-silver configurations were designed to test the strain-sensitivity performance of both graphite-PDMS and Ag-PDMS composites individually. Both sensors were printed using similar G-code scripts, where only the infill of the pads was modified based on the material used. A larger infill separation is specified for silver because the ink exhibits a larger spread.

The graphite-silver hybrid sensor was designed as silver has a higher conductivity than graphite and is suitable for wiring and connections, whereas graphite is more strain-sensitive. Therefore, the configuration was designed to examine the effect of using a combination of both materials on the sensor performance. Printing of this sensor was more complex as it required the use of dual extruders to print with two inks in a single operation. This required a thorough calibration process.

The configurations presented above were printed using the Allevi 2. Images of the final strain gauge sensor products are shown in figure 9. The print parameters used are shown in table 2.

Print parameter	Graphite-PDMS	Ag-PDMS
Extruding nozzle diameter (AWG)	27	32
Extruding pressure (psi)	9.5	6.5
Print speed (mms^{-1})	10	10

Table 2: Print parameters for sensor configurations

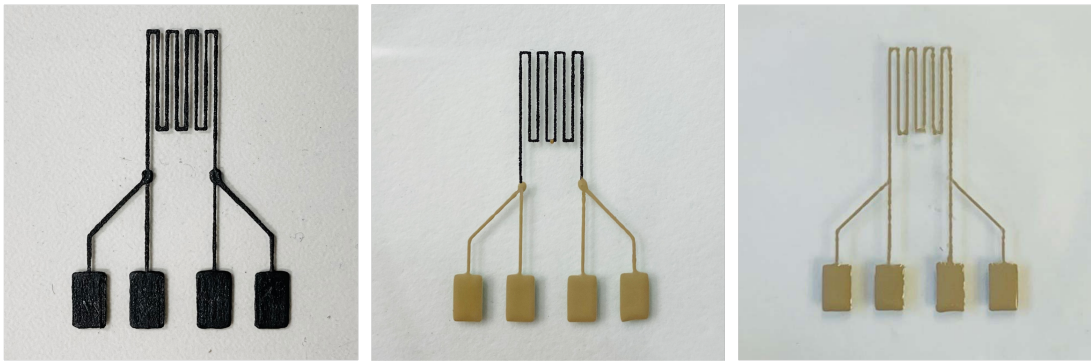


Figure 9: Fabricated strain gauge sensors

2.7 Experimental Procedure

2.7.1 Preparation

To measure the device's electrical resistance, wires were attached to the four pads of the sensor using silver paste (product no. 186-3600). The wires were placed on the pads and silver paste was deposited and this was placed on a hot plate for around 15 minutes to ensure curing of the paste. Another layer was then applied and heated for a further 15 minutes. To ensure secure attachment of the wires, insulating tape was wrapped around the pads. The wires were then connected to a Keithley 4200A-SCS Parameter Semiconductor Analyser which measures the four-point resistance of the sensor. To assess the performance, we measure the resistance of the sensor against two different forms of strain; stretching and bending. Only the all-graphite sensor configuration was tested due to encountered problems with Ag-PDMS that is discussed in section 5.1.

2.7.2 Testing procedure for stretching

The parameters of equation 1 are required to assess the performance of the sensor. A custom-built setup provided [39] was used to measure these parameters and is shown in figure 10. The sensor is connected to the semiconductor analyser and is placed between two clamps to be stretched via the moving platform. The force meter measures the force of stretching, and a caliper measures the elongation corresponding to each force. Prior to testing/stretching, the initial resistance was measured.

The sensor was stretched at intervals of 0.2 N from 0–2 N. The elongation was recorded for each value of force. At each interval, the resistance of the device was measured using the impedance analyser. A current of $20 \mu\text{A}$ was injected between the outer two pads, and the remaining two probes measured the voltage across the two inner pads. The four-point resistance is therefore calculated accordingly. For each interval, 100 samples of the resistance were calculated at 0.5s intervals. This process was repeated three times. The data from the analyser was extracted, averaged and plotted, this is presented in section 3.2.

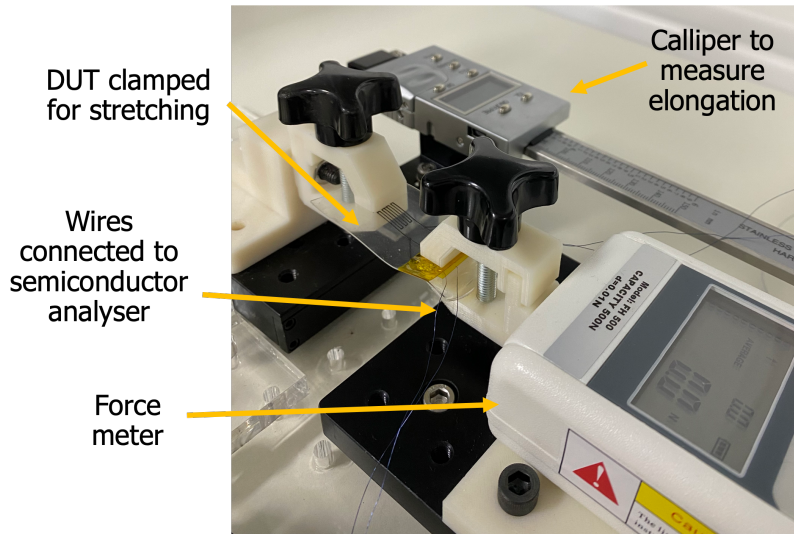


Figure 10: Experimental setup for resistance versus stretching test

2.7.3 Testing procedure for bending

For the resistance versus bending test, 3D printed arc fixtures of different radii were used to bend the sensor. Figure 11 shows the fixtures as well as their radii. The sensor is placed in each fixture and the resistance is measured (100 samples at 1s intervals). Due to the hysteresis nature of the resistance variation, between each fixture measurement, a settling time of around three minutes is allowed before taking the next set of measurements to ensure accurate results. The same method of calculating the four-point resistance in the previous test was followed. As previously, the data from the analyser was extracted and plotted, this is also presented in section 3.2. The bending test was only performed once due to time constraints.

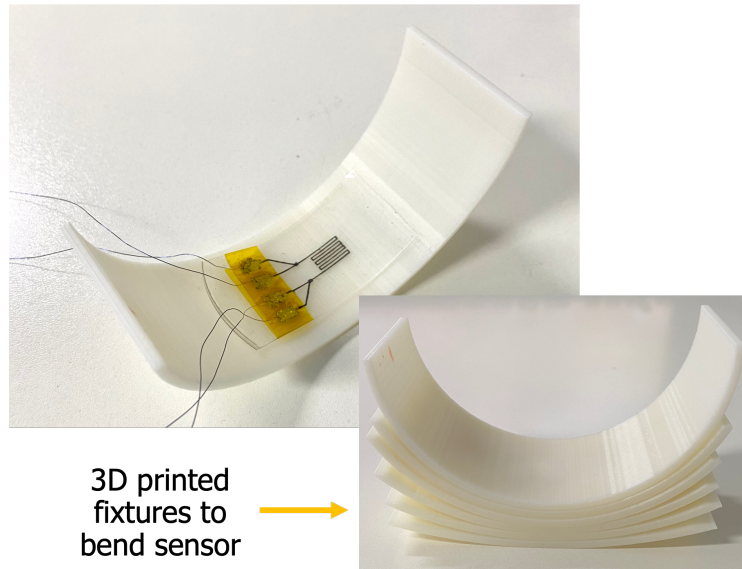


Figure 11: Experimental setup for resistance versus bending test

3 Results

3.1 Characterisation of Printed Lines

Figure 13 shows the results of the characterisation process described in section 2.5.1 for the graphite ink. The first plot captures the variation of the track width against the extruding pressure, whilst the second plot captures the variation against the print speed. Figure 14 shows identical plots for the Ag-PDMS ink. The average minimum resolution achieved was approximately 105 μm . This is shown in figure 12.

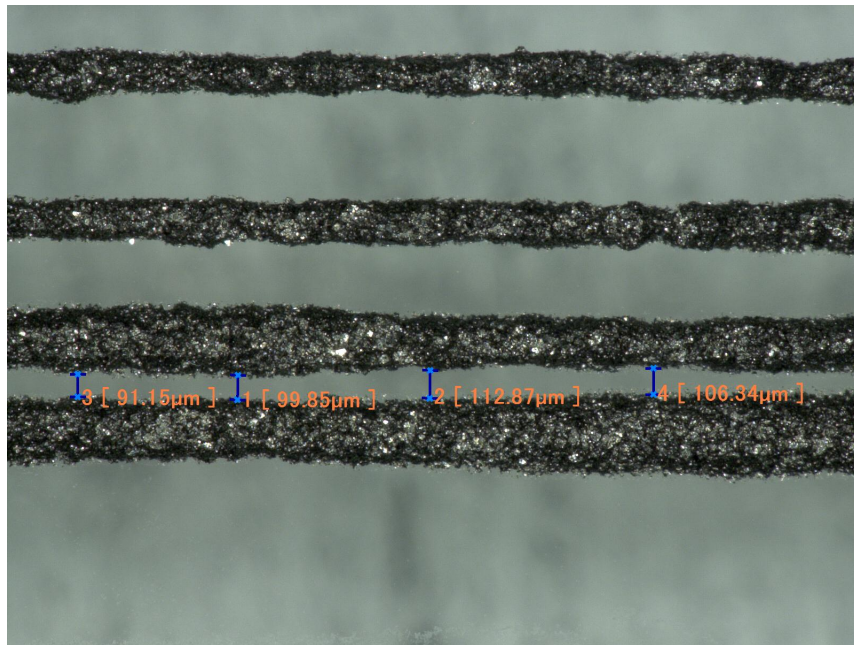


Figure 12: Graphite tracks under microscope

Error bars are computed and plotted, however various measurements are associated with a small error and for this reason, the corresponding error bars are not clearly visualised. The data was fitted to a linear function, where the line equation and the R^2 value (coefficient of determination) is shown.

3.2 Characterisation of Sensors

3.2.1 Stretching

Resistance variation range

Firstly, the resistance variation of the strain gauge sensor with stretching, plotted against both elongation (figure 15) and force (figure 17). Figure 16 shows the elongation plot with error bars. These plots show the range of resistance values the sensor reaches when being stretched.

Gauge factor

To compute the gauge factor, the normalised change in resistance is plotted against

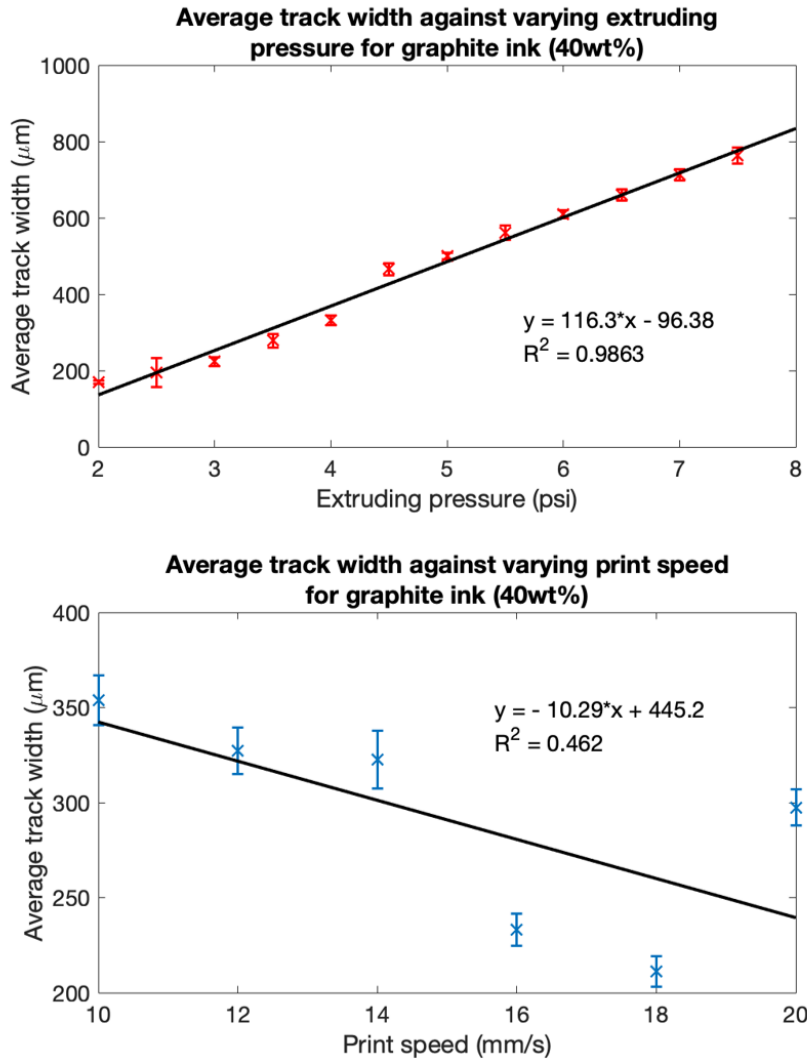


Figure 13: Pressure and speed characterisation results for graphite-PDMS ink

the applied strain, presented in figure 18. A linear fit was computed, where the equation of the line and the R^2 value is shown. According to equation 1, the gauge factor is the gradient of this line. Figure 19 shows the same plot with error bars.

3.2.2 Bending

The results from section 2.7.3 are presented in figure 20 to assess the performance of the sensor against different radii of bending.

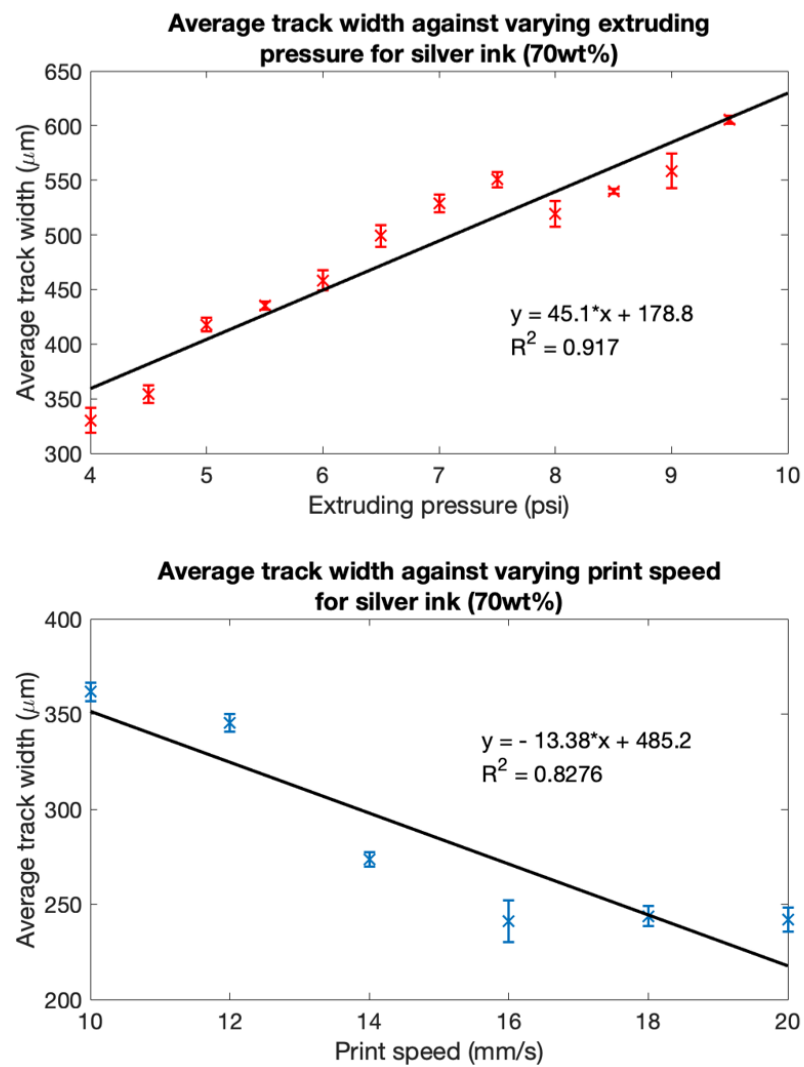


Figure 14: Pressure and speed characterisation results for Ag-PDMS ink

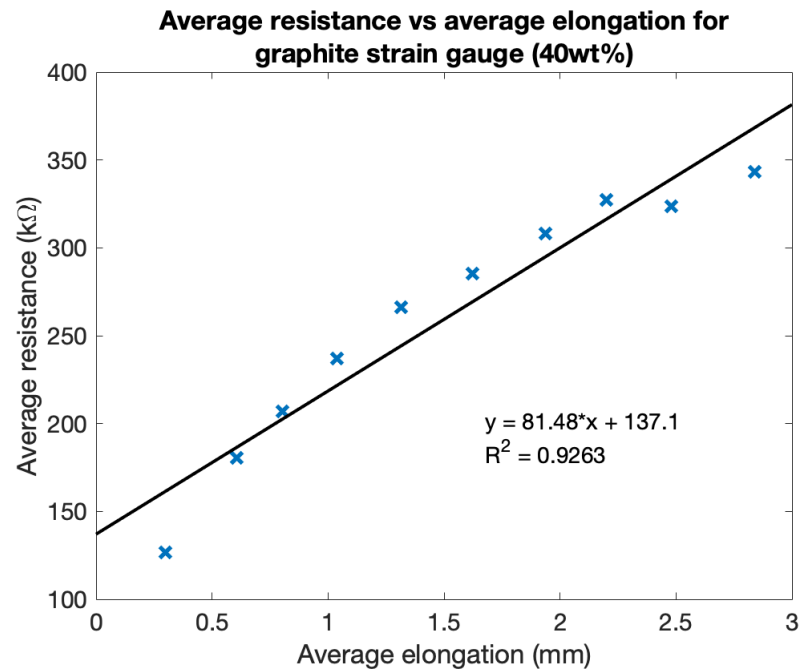


Figure 15: Resistance variation with elongation

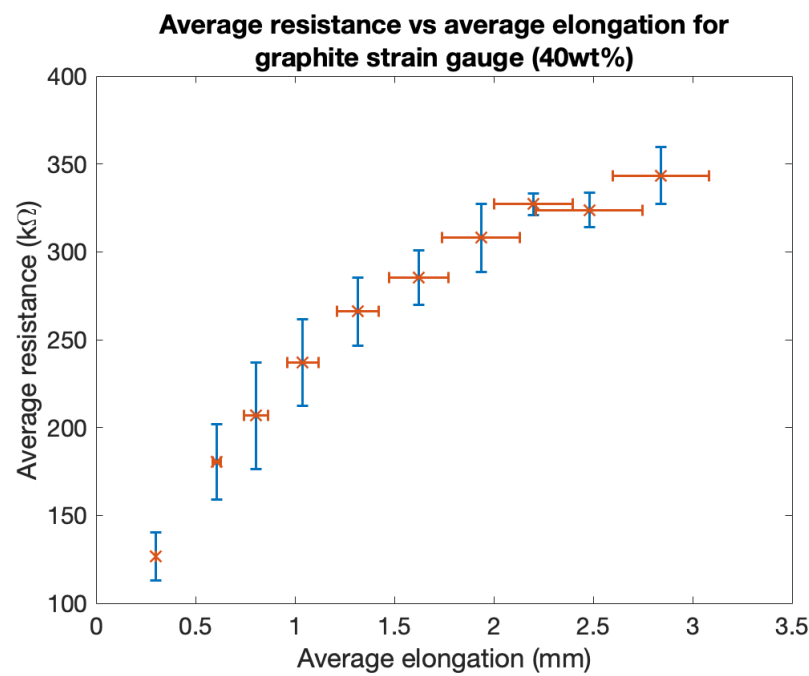


Figure 16: Resistance variation with elongation (error bars)

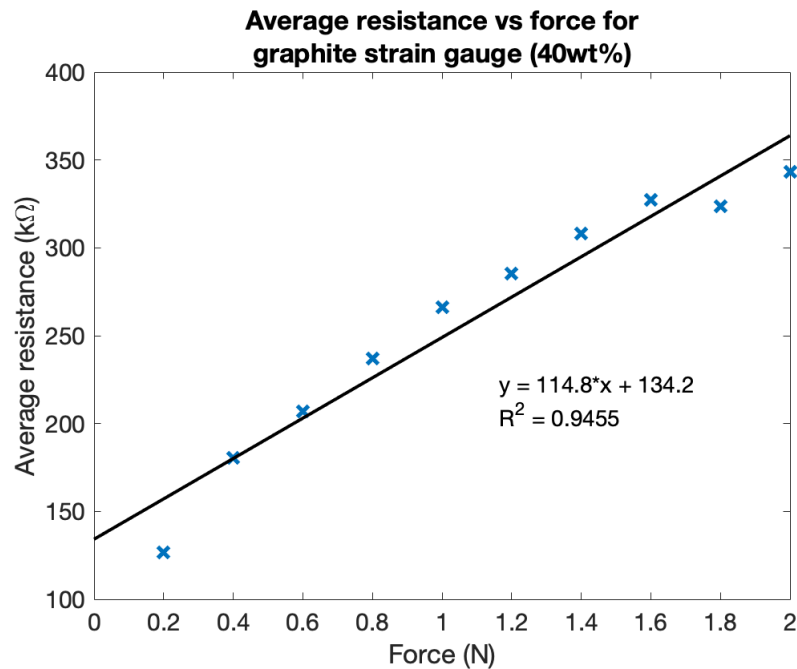


Figure 17: Resistance variation with force

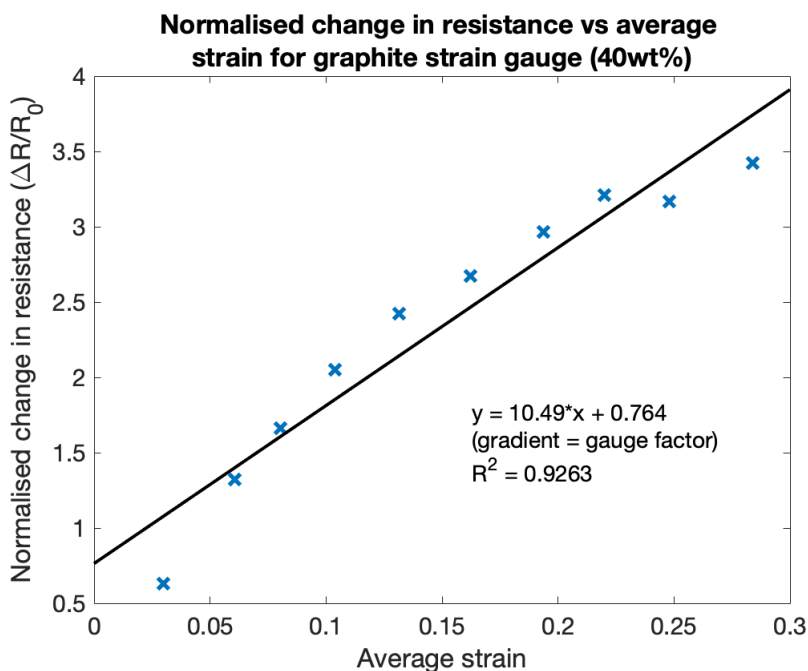


Figure 18: Normalised change in resistance against applied strain

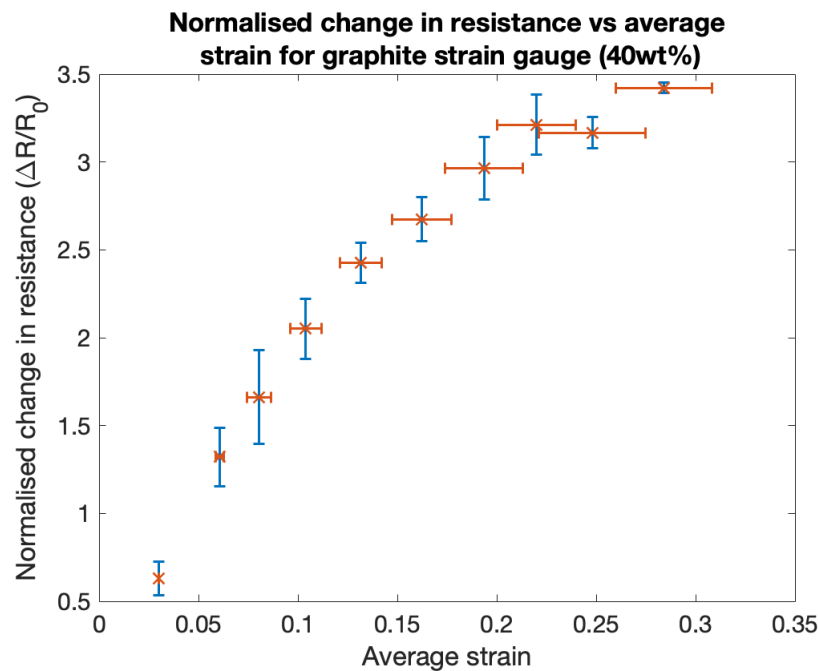


Figure 19: Normalised change in resistance against applied strain (with error bars)

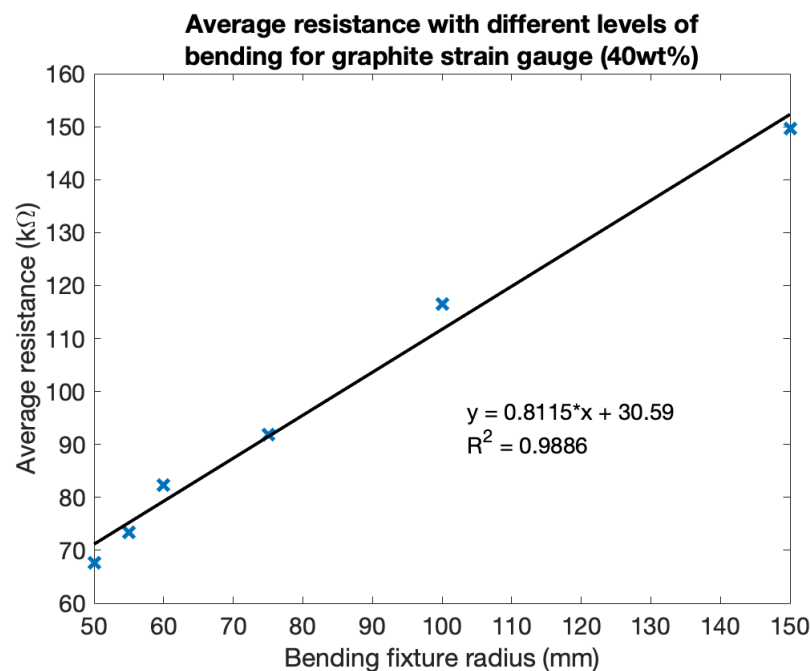


Figure 20: Normalised change in resistance against different radii of bending

4 Discussion

4.1 Characterisation of Printed Lines

4.1.1 Track width versus pressure

The results in section 3.1 show that, as expected, the track width increases with extruding pressure. This is for both the graphite- and Ag-PDMS inks. From the graphs, we observe that the average track width for Ag-PDMS starts at a larger value of approximately $350 \mu\text{m}$ compared to that of graphite-PDMS (approximately $200 \mu\text{m}$). This might seem counter-intuitive since a smaller needle diameter was used for silver inks, leading to the expectation that the silver tracks would be of a smaller width. However, the opposite occurs due to the heavier weight of the silver particles, which causes a larger ink spread post-printing. The minimum extruding pressure for the defined recipe of graphite-PDMS ink was 2 psi. For Ag-PDMS this value is 4 psi and this is expected to be higher than that for graphite as a smaller needle diameter is used.

4.1.2 Track width versus speed

The track width also decreases with a higher print speed, which is again the expected scenario. In this case, there is larger variation in track width when compared to the pressure plots. The reason for this is due to limited printer capabilities, where only a small speed range is recommended. In this project the printer was tested at its limits and at higher speeds becomes increasingly inconsistent.

The characterisation process will hence allow users of the Allevi 2 printer to effortlessly choose a suitable extruding pressure and print speed depending on the required print geometries and sensor application.

4.2 Characterisation of the Sensor

4.2.1 Stretching

The key parameters measured/computed are summarised in table 3. As expected, the resistance of the device increases with increased strain, as observed from figure 15 or 17. The resistance increase appears to be linear with a linear fit R^2 value of 0.92. From 18 we can see linearity indicating a constant gauge factor of 10.49. However, this might not be the case when testing with larger strains and so further testing would be required. Figure 19 shows small vertical error bars (for resistance) indicating good repeatability of results. As a comparison, strain gauge sensors from other approaches are reviewed in table 4. Since not many graphite-PDMS strain sensors were found in the literature, carbon and graphene based composites are used as an alternative for the comparison.

From the literature we observe that most stretchable strain gauges have a gauge factor ranging from approximately 0.5–4 with some with higher values of 29 such as

Parameter	Value
Initial resistance	78 kΩ
Resistance variation range	78–343 kΩ
Gauge factor	10.49

Table 3: Summary of measured/computed parameters

Reference	Base resistance	Material	Print method	Gauge factor
[17]	4.13 MΩ	CB-PDMS	Photoresist patterning	29.1
[17]	0.31 MΩ	CNT-PDMS	Photoresist patterning	0.52
[18]	60 kΩ	Carbon conductive grease	Embedded 3D printing	3.8±0.6
[40]	—	CNT-Ecoflex	Embedded 3D printing	3.4
[15]	—	MWCNT-PDMS	3D printing	4.3
This work	78 kΩ	Graphite-PDMS	3D printing	10.49

Table 4: Comparing different fabricated strain gauge sensors

[17]. For a strain gauge sensor demonstration, a gauge factor of 10.49 is exceptional. The effect of the sensor geometry on strain sensitivity was not considered, therefore with a more carefully studied approach for the geometries a higher gauge factor can potentially be achieved.

4.2.2 Bending

From figure 20 we can see that with decreased bending radius, i.e. more bending, the sensor resistance decreases. Other approaches exhibit the same but present it vice versa as the type of bending may vary (inward/outward bending). In this case, the sensor is bent inwards (see 11. This causes the graphite particles to be closer in proximity and therefore more percolation networks are introduced, therefore causing increased conductance hence decreased resistance. When bent, parts of the graphite will be closer while other parts will be further away. The overall effect will be determined by which of these dominates. in the case of inward bending, it is safe to assume that more graphite particles are pushed closer together. Other approaches in [15, 18, 40] bend the sensor outwards and this causes the opposite effect. The strain sensor demonstrated here has not been tested when bent in the opposite direction due to time constraints, but it would be sensible to assume it would exhibit the opposite effect.

Therefore, we observe that the sensor can be used to implement human motion monitoring (such as wrist/finger/joint flexion/extension) or in soft robotics as pressure/force sensors.

5 Conclusion

5.1 Future Work

5.1.1 Further testing for all-graphite sensor

The graphite sensor requires further testing in order to fully characterise its properties and performance. Firstly, tests for stretching will need to be repeated at higher forces/strains in order to determine the gauge factor behaviour; whether it will remain linear or exhibit quadratic behaviour. The next test that needs to be performed is a hysteresis test to determine the settling time of the sensor back to its initial/base resistance value.

5.1.2 Testing for all-silver and graphite-silver hybrid sensors

The next steps include testing the remaining two configurations to assess the strain sensitivity of Ag-PDMS inks and how the combination of both inks affects sensor performance. In order to establish a successful electrical connection, it is recommended to try an approach where prior to printing, the wires are placed and secured on the Petri dish at the pad locations, where printing is then started. This will result in the ink being directly printed onto the wires, therefore after curing, a secure connection should be established. This should ideally ensure an electrical connection even if the silver particles deposit at the bottom of the pads.

5.1.3 Develop a fully stretchable multiparameter sensing system

After demonstrating and assessing the behaviour of the inks (separately and as a hybrid) in a strain gauge sensor, future work can include fabricating different types of sensors such as temperature, ECG, bioimpedance etc. These individual sensors can then be integrated in a single multiparameter system that can be implemented in wearables or soft robotics. This is inspired by the flexible multiparametric sensing system presented by Kassanos et al. [6].

5.1.4 Embedded printing in uncured PDMS

An interesting area in stretchable electronics is printing within an uncured elastomer matrix in order to fabricate sensors enclosed within the elastomer to offer protection of the sensor. Soft PCBs are becoming increasingly popular, and with embedded printing, multi-layer prints can be realised, complemented by the use of 3D printing. An example is shown in [41] but this approach is not fabricated using 3D printing.

5.2 Summary

The optimisation and characterisation of the printing parameters using custom-fabricated graphite- and Ag-PDMS inks was presented. This yielded the printing of different geometries and structures, where eventually a strain gauge sensor demo was realised. Resistance variation with applied strain is shown for the all-graphite

sensor configuration. The sensor demonstrated typical strain gauge behaviour with a gauge factor of 6.94, although further testing is required to compute this at higher levels of strain. The sensor can be implemented as a force/bending sensor for human motion monitoring or as an e-skin for soft robotics. Further testing has been suggested to better characterise the sensor, as well as future developments that can be made regarding the project.

The remaining two configurations (all-silver and graphite-silver hybrid) exhibited problems with testing, where it is suspected that the silver particles deposit at the bottom leaving an insulating layer of PDMS at the top thus preventing a successful electrical connection. Further investigation is required in the silver-PDMS ink fabrication process.

References

- [1] D. Zhang, T. Huang, and L. Duan, “Emerging Self-Emissive Technologies for Flexible Displays,” *Advanced Materials*, vol. 32, no. 15, p. 1902391, 2020. 1
- [2] J. H. Koo, D. C. Kim, H. J. Shim, T.-H. Kim, and D.-H. Kim, “Flexible and Stretchable Smart Display: Materials, Fabrication, Device Design, and System Integration,” *Advanced Functional Materials*, vol. 28, no. 35, p. 1801834, 2018. 1
- [3] R. P. Rocha, P. A. Lopes, A. T. de Almeida, M. Tavakoli, and C. Majidi, “Fabrication and Characterization of Bending and Pressure Sensors for a Soft Prosthetic Hand,” *Journal of Micromechanics and Microengineering*, vol. 28, no. 3, p. 034001, 2018. 1, 2
- [4] J. C. Yeo, H. K. Yap, W. Xi, Z. Wang, C.-H. Yeow, and C. T. Lim, “Flexible and Stretchable Strain Sensing Actuator for Wearable Soft Robotic Applications,” *Advanced Materials Technologies*, vol. 1, no. 3, p. 1600018, 2016. 1
- [5] K. Keum, J. W. Kim, S. Y. Hong, J. G. Son, S.-S. Lee, and J. S. Ha, “Flexible/Stretchable Supercapacitors with Novel Functionality for Wearable Electronics,” *Advanced Materials*, vol. 32, no. 51, p. 2002180, 2020. 1
- [6] P. Kassanos, F. Seichepine, D. Wales, and G.-Z. Yang, “Towards a Flexible/Stretchable Multiparametric Sensing Device for Surgical and Wearable Applications,” in *2019 IEEE Biomedical Circuits and Systems Conference (BioCAS)*, 2019, pp. 1–4. 1, 23
- [7] W.-P. Shih, L.-C. Tsao, C.-W. Lee, M.-Y. Cheng, C. Chang, Y.-J. Yang, and K.-C. Fan, “Flexible Temperature Sensor Array Based on a Graphite-Polydimethylsiloxane Composite,” *Sensors*, vol. 10, no. 4, pp. 3597–3610, 2010. 1
- [8] J. Guo, B. Zhou, C. Yang, Q. Dai, and L. Kong, “Stretchable and Temperature-Sensitive Polymer Optical Fibers for Wearable Health Monitoring,” *Advanced Functional Materials*, vol. 29, no. 33, p. 1902898, 2019.
- [9] H. Xu, Y. Lv, D. Qiu, Y. Zhou, H. Zeng, and Y. Chu, “An Ultra-Stretchable, Highly Sensitive and Biocompatible Capacitive Strain Sensor from an Ionic Nanocomposite for On-Skin Monitoring,” *Nanoscale*, vol. 11, pp. 1570–1578, 2019.
- [10] J. Kim and W. S. Kim, “A Paired Stretchable Printed Sensor System for Ambulatory Blood Pressure Monitoring,” *Sensors and Actuators A: Physical*, vol. 238, pp. 329–336, 2016. 1
- [11] H.-S. Chuang and S. Wereley, “Design, Fabrication and Characterization of a Conducting PDMS for Microheaters and Temperature Sensors,” *Journal of Micromechanics and Microengineering*, vol. 19, no. 4, p. 045010, 2009. 1

- [12] A. J. Bandodkar, I. Jeerapan, J.-M. You, R. Nuñez-Flores, and J. Wang, "Highly Stretchable Fully-Printed CNT-Based Electrochemical Sensors and Bio-fuel Cells: Combining Intrinsic and Design-Induced Stretchability," *Nano Letters*, vol. 16, no. 1, pp. 721–727, 2016. 1
- [13] A. J. Bandodkar, R. Nuñez-Flores, W. Jia, and J. Wang, "All-Printed Stretchable Electrochemical Devices," *Advanced Materials*, vol. 27, no. 19, pp. 3060–3065, 2015. 1
- [14] S. Y. Oh, S. Y. Hong, Y. R. Jeong, J. Yun, H. Park, S. W. Jin, G. Lee, J. H. Oh, H. Lee, S.-S. Lee, and J. S. Ha, "Skin-Attachable, Stretchable Electrochemical Sweat Sensor for Glucose and pH Detection," *ACS Applied Materials & Interfaces*, vol. 10, no. 16, pp. 13 729–13 740, 2018. 1
- [15] M. Abshirini, M. Charara, Y. Liu, M. Saha, and M. C. Altan, "3d printing of highly stretchable strain sensors based on carbon nanotube nanocomposites," *Advanced Engineering Materials*, vol. 20, no. 10, p. 1800425, 2018. 1, 22
- [16] W. B. Dobie and P. C. G. Isaac, "Electric Resistance Strain Gauges," *The Journal of the Royal Aeronautical Society*, vol. 53, no. 458, p. 189–189, 1949. 2
- [17] N. Lu, C. Lu, S. Yang, and J. Rogers, "Highly Sensitive Skin-Mountable Strain Gauges Based Entirely on Elastomers," *Advanced Functional Materials*, vol. 22, no. 19, pp. 4044–4050, 2012. 2, 22
- [18] J. T. Muth, D. M. Vogt, R. L. Truby, Y. Mengüç, D. B. Kolesky, R. J. Wood, and J. A. Lewis, "Embedded 3D Printing of Strain Sensors within Highly Stretchable Elastomers," *Advanced Materials*, vol. 26, no. 36, pp. 6307–6312, 2014. 2, 22
- [19] Z. Wang, Q. Zhang, Y. Yue, J. Xu, W. Xu, X. Sun, Y. Chen, J. Jiang, and Y. Liu, "3D Printed Graphene/Polydimethylsiloxane Composite for Stretchable Strain Sensor with Tunable Sensitivity," *Nanotechnology*, vol. 30, no. 34, p. 345501, 2019. 2
- [20] S. Han Min, A. Asrulnizam, M. Atsunori, and M. Mariatti, "Properties of Stretchable and Flexible Strain Sensor Based on Silver/PDMS Nanocomposites," *Materials Today: Proceedings*, vol. 17, pp. 616–622, 2019, 6th International Conference on Recent Advances in Materials, Minerals & Environment (RAMM) 2018, RAMM 2018, 27 - 29 November 2018, Penang, Malaysia. 2
- [21] J. F. Christ, N. Aliheidari, P. Pötschke, and A. Ameli, "Bidirectional and stretchable piezoresistive sensors enabled by multimaterial 3d printing of carbon nanotube/thermoplastic polyurethane nanocomposites," *Polymers*, vol. 11, no. 1, 2019. 2
- [22] M. Amjadi, K.-U. Kyung, I. Park, and M. Sitti, "Stretchable, Skin-Mountable, and Wearable Strain Sensors and Their Potential Applications: A Review," *Advanced Functional Materials*, vol. 26, no. 11, pp. 1678–1698, 2016. 2

- [23] M.-Y. Cheng, C.-M. Tsao, and Y.-J. Yang, “An Anthropomorphic Robotic Skin Using Highly Twistable Tactile Sensing Array,” in *2010 5th IEEE Conference on Industrial Electronics and Applications*, 2010, pp. 650–655. 2
- [24] Y. Maithani, B. Choudhuri, B. Mehta, and J. Singh, “Self-Adhesive, Stretchable, and Dry Silver Nanorods Embedded Polydimethylsiloxane Biopotential Electrodes for Electrocardiography,” *Sensors and Actuators A: Physical*, vol. 332, p. 113068, 2021. 2
- [25] A. Larmagnac, S. Eggenberger, H. Janossy, and J. Vörös, “Stretchable Electronics Based on Ag-PDMS Composites,” *Scientific reports*, vol. 4, p. 7254, 12 2014. 2, 4
- [26] D. McCoul, W. Hu, M. Gao, V. Mehta, and Q. Pei, “Recent Advances in Stretchable and Transparent Electronic Materials,” *Advanced Electronic Materials*, vol. 2, no. 5, p. 1500407, 2016. 2
- [27] D. F. Fernandes, C. Majidi, and M. Tavakoli, “Digitally printed stretchable electronics: a review,” *J. Mater. Chem. C*, vol. 7, pp. 14 035–14 068, 2019. 2
- [28] Z. Wang, W. Gao, Q. Zhang, K. Zheng, J. Xu, W. Xu, E. Shang, J. Jiang, J. Zhang, and Y. Liu, “3D-Printed Graphene/Polydimethylsiloxane Composites for Stretchable and Strain-Insensitive Temperature Sensors,” *ACS Applied Materials & Interfaces*, vol. 11, no. 1, pp. 1344–1352, 2019. 3
- [29] R. Zheng, Y. Chen, H. Chi, H. Qiu, H. Xue, and H. Bai, “3d printing of a polydimethylsiloxane/polytetrafluoroethylene composite elastomer and its application in a triboelectric nanogenerator,” *ACS Applied Materials & Interfaces*, vol. 12, no. 51, pp. 57 441–57 449, 12 2020. 3
- [30] Z. Wang, Q. Zhang, Y. Yue, J. Xu, W. Xu, X. Sun, Y. Chen, J. Jiang, and Y. Liu, “3D Printed Graphene/Polydimethylsiloxane Composite for Stretchable Strain Sensor with Tunable Sensitivity,” *Nanotechnology*, vol. 30, no. 34, p. 345501, 2019. [Online]. Available: <https://doi.org/10.1088/1361-6528/ab1287> 3
- [31] I. S. Yoon, Y. Oh, S. H. Kim, J. Choi, Y. Hwang, C. H. Park, and B.-K. Ju, “3D Printing of Self-Wiring Conductive Ink with High Stretchability and Stackability for Customized Wearable Devices,” *Advanced Materials Technologies*, vol. 4, no. 9, p. 1900363, 2019. 3
- [32] M. Hu, P. Kassanos, M. Keshavarz, E. Yeatman, and B. Lo, “Electrical and Mechanical Characterization of Carbon-Based Elastomeric Composites for Printed Sensors and Electronics,” in *2021 IEEE International Conference on Flexible and Printable Sensors and Systems (FLEPS)*, 2021, pp. 1–4. 3, 4, 7
- [33] J. C. Lötters, W. Olthuis, P. H. Veltink, and P. Bergveld, “The Mechanical Properties of the Rubber Elastic Polymer Polydimethylsiloxane for Sensor Applications,” *Journal of Micromechanics and Microengineering*, vol. 7, no. 3, pp. 145–147, 1997. 4

- [34] M. E. Spahr, R. Gilardi, and D. Bonacchi, *Carbon Black for Electrically Conductive Polymer Applications*. Springer Berlin Heidelberg, 2021, pp. 1–20. 4
- [35] A. B. Oskouyi, U. Sundararaj, and P. Mertiny, “Tunneling Conductivity and Piezoresistivity of Composites Containing Randomly Dispersed Conductive Nano-Platelets,” *Materials*, vol. 7, no. 4, pp. 2501–2521, 2014. 4
- [36] X. Niu, S. Peng, L. Liu, W. Wen, and P. Sheng, “Characterizing and Patterning of PDMS-Based Conducting Composites,” *Advanced Materials*, vol. 19, no. 18, pp. 2682–2686, 2007. 4
- [37] S. Stassi, V. Cauda, G. Canavese, and C. F. Pirri, “Flexible Tactile Sensing Based on Piezoresistive Composites: A Review,” *Sensors*, vol. 14, no. 3, pp. 5296–5332, 2014. 5
- [38] S. Agarwala, G. L. Goh, Y. L. Yap, G. D. Goh, H. Yu, W. Y. Yeong, and T. Tran, “Development of bendable strain sensor with embedded microchannels using 3d printing,” *Sensors and Actuators A: Physical*, vol. 263, pp. 593–599, 2017. 9
- [39] P. Kassanos, G.-Z. Yang, and E. Yeatman, “An Interdigital Strain Sensor Through Laser Carbonization of PI and PDMS Transfer,” in *2021 IEEE International Conference on Flexible and Printable Sensors and Systems (FLEPS)*, 2021, pp. 1–4. 13
- [40] B. Herren, M. C. Saha, M. C. Altan, and Y. Liu, “Development of ultrastretchable and skin attachable nanocomposites for human motion monitoring via embedded 3D printing,” *Composites Part B: Engineering*, vol. 200, p. 108224, 2020. [Online]. Available: <https://www.sciencedirect.com/science/article/pii/S1359836820332741> 22
- [41] X. Niu, S. Peng, L. Liu, W. Wen, and P. Sheng, “Characterizing and patterning of pdms-based conducting composites,” *Advanced Materials*, vol. 19, no. 18, pp. 2682–2686, 2007. 23

A G-Code Scripts

A.1 All-graphite-PDMS G-code script

```
; strain gauge sensor gcode for 1 ink (graphite)

; initialisation
G28 ; home all axes
G1 Z5 F ; lift nozzle

; extruder selection
; T0 = extruder 1, T1 = extruder 2
T0

; set up
G21 ; set units to millimeters
G90 ; use absolute coordinates
M82 ; use absolute distances for extrusion
G92 E0

G1 Z0.08 F360 ; layer height
G1 F540 ; print speed 9mm/s

; strain gauge sensing element
; using extruder 1 - graphite ink
G1 X-3.5 Y-16 ; wire 1
G1 X-3.5 Y10 E0.01
G1 X-2.5 Y10 E0.02
G1 X-2.5 Y0 E0.03
G1 X-1.5 Y0 E0.04
G1 X-1.5 Y10 E0.05
G1 X-0.5 Y10 E0.06
G1 X-0.5 Y0 E0.07
G1 X0.5 Y0 E0.08
G1 X0.5 Y10 E0.09
G1 X1.5 Y10 E0.10
G1 X1.5 Y0 E0.11
G1 X2.5 Y0 E0.12
G1 X2.5 Y10 E0.13
G1 X3.5 Y10 E0.14
G1 X3.5 Y-16 E0.15 ; wire 4
G92 E0

; connecting pads and wires 3-4
G1 X3.75 Y-4.5
G1 Z0.080 F360 ; return to layer height
```

```
G1 F360
G1 X3.75 Y-4.5 E0.01
G1 X3.75 Y-5.25 E0.02
G1 X3.25 Y-5.25 E0.03
G1 X3.25 Y-4.5 E0.04
G1 X3.75 Y-4.5 E0.05
G92 E0
G1 X3.5 Y-4.5
G1 X3.5 Y-5 E0.01

; wire 4
G1 X9.5 Y-11 E0.02
G1 X9.5 Y-15 E0.03

; pad 4
G1 X11 Y-15 E0.04
G1 X11 Y-20 E0.05
G1 X8 Y-20 E0.06
G1 X8 Y-15 E0.07
G1 X9.5 Y-15 E0.08
G92 E0
G1 F540
G1 X10.8 Y-20 ; pad infill
G1 X10.8 Y-15 E0.01
G1 X10.6 Y-15 E0.02
G1 X10.6 Y-20 E0.03
G1 X10.4 Y-20 E0.04
G1 X10.4 Y-15 E0.05
G1 X10.2 Y-15 E0.06
G1 X10.2 Y-20 E0.07
G1 X10.0 Y-20 E0.08
G1 X10.0 Y-15 E0.09
G1 X9.8 Y-15 E0.10
G1 X9.8 Y-20 E0.11
G1 X9.6 Y-20 E0.12
G1 X9.6 Y-15 E0.13
G1 X9.4 Y-15 E0.14
G1 X9.4 Y-20 E0.15
G1 X9.2 Y-20 E0.16
G1 X9.2 Y-15 E0.17
G1 X9.0 Y-15 E0.18
G1 X9.0 Y-20 E0.19
G1 X8.8 Y-20 E0.20
G1 X8.8 Y-15 E0.21
G1 X8.6 Y-15 E0.22
```

```
G1 X8.6 Y-20 E0.23
G1 X8.4 Y-20 E0.24
G1 X8.4 Y-15 E0.25
G1 X8.2 Y-15 E0.26
G1 X8.2 Y-20 E0.27
G1 X8.0 Y-20 E0.28
G1 X8.0 Y-15 E0.29
G92 E0
G1 Z1 F360 ; lower bedplate

; pad 3
G1 X3.5 Y-15
G1 F360
G1 Z0.080 F360 ; return to layer height
G1 X5 Y-15 E0.01
G1 X5 Y-20 E0.02
G1 X2 Y-20 E0.03
G1 X2 Y-15 E0.04
G1 X2 Y-15 E0.05
G1 X3.5 Y-15 E0.06
G92 E0
G1 F540
G1 X4.8 Y-20 ; pad infill
G1 X4.8 Y-15 E0.01
G1 X4.6 Y-15 E0.02
G1 X4.6 Y-20 E0.03
G1 X4.4 Y-20 E0.04
G1 X4.4 Y-15 E0.05
G1 X4.2 Y-15 E0.06
G1 X4.2 Y-20 E0.07
G1 X4.0 Y-20 E0.08
G1 X4.0 Y-15 E0.09
G1 X3.8 Y-15 E0.10
G1 X3.8 Y-20 E0.11
G1 X3.6 Y-20 E0.12
G1 X3.6 Y-15 E0.13
G1 X3.4 Y-15 E0.14
G1 X3.4 Y-20 E0.15
G1 X3.2 Y-20 E0.16
G1 X3.2 Y-15 E0.17
G1 X3.0 Y-15 E0.18
G1 X3.0 Y-20 E0.19
G1 X2.8 Y-20 E0.20
G1 X2.8 Y-15 E0.21
G1 X2.6 Y-15 E0.22
```

```
G1 X2.6 Y-20 E0.23
G1 X2.4 Y-20 E0.24
G1 X2.4 Y-15 E0.25
G1 X2.2 Y-15 E0.26
G1 X2.2 Y-20 E0.27
G1 X2.0 Y-20 E0.28
G1 X2.0 Y-15 E0.29
G92 E0
G1 Z1 F360 ; lower bedplate

; connecting pads and wires 1-2
G1 X-3.75 Y-4.5
G1 Z0.080 F360 ; return to layer height
G1 F360
G1 X-3.75 Y-4.5 E0.01
G1 X-3.75 Y-5.25 E0.02
G1 X-3.25 Y-5.25 E0.03
G1 X-3.25 Y-4.5 E0.04
G1 X-3.75 Y-4.5 E0.05
G92 E0
G1 X-3.5 Y-4.5
G1 X-3.5 Y-5 E0.01

; wire 1
G1 X-9.5 Y-11 E0.02
G1 X-9.5 Y-15 E0.03

; pad 1
G1 X-11 Y-15 E0.04
G1 X-11 Y-20 E0.05
G1 X-8 Y-20 E0.06
G1 X-8 Y-15 E0.07
G1 X-9.5 Y-15 E0.08
G92 E0
G1 F540
G1 X-10.8 Y-20 ; pad infill
G1 X-10.8 Y-15 E0.01
G1 X-10.6 Y-15 E0.02
G1 X-10.6 Y-20 E0.03
G1 X-10.4 Y-20 E0.04
G1 X-10.4 Y-15 E0.05
G1 X-10.2 Y-15 E0.06
G1 X-10.2 Y-20 E0.07
G1 X-10.0 Y-20 E0.08
G1 X-10.0 Y-15 E0.09
```

```

G1 X-9.8 Y-15 E0.10
G1 X-9.8 Y-20 E0.11
G1 X-9.6 Y-20 E0.12
G1 X-9.6 Y-15 E0.13
G1 X-9.4 Y-15 E0.14
G1 X-9.4 Y-20 E0.15
G1 X-9.2 Y-20 E0.16
G1 X-9.2 Y-15 E0.17
G1 X-9.0 Y-15 E0.18
G1 X-9.0 Y-20 E0.19
G1 X-8.8 Y-20 E0.20
G1 X-8.8 Y-15 E0.21
G1 X-8.6 Y-15 E0.22
G1 X-8.6 Y-20 E0.23
G1 X-8.4 Y-20 E0.24
G1 X-8.4 Y-15 E0.25
G1 X-8.2 Y-15 E0.26
G1 X-8.2 Y-20 E0.27
G1 X-8.0 Y-20 E0.28
G1 X-8.0 Y-15 E0.29
G92 E0
G1 Z1 F360 ; lower bedplate

; pad 2
G1 X-3.5 Y-15
G1 Z0.080 F360 ; return to layer height
G1 F360
G1 X-5 Y-15 E0.02
G1 X-5 Y-20 E0.03
G1 X-2 Y-20 E0.04
G1 X-2 Y-15 E0.05
G1 X-2 Y-15 E0.06
G1 X-3.5 Y-15 E0.07
G92 E0
G1 F540
G1 X-4.8 Y-20 ; pad infill
G1 X-4.8 Y-15 E0.01
G1 X-4.6 Y-15 E0.02
G1 X-4.6 Y-20 E0.03
G1 X-4.4 Y-20 E0.04
G1 X-4.4 Y-15 E0.05
G1 X-4.2 Y-15 E0.06
G1 X-4.2 Y-20 E0.07
G1 X-4.0 Y-20 E0.08
G1 X-4.0 Y-15 E0.09

```

```
G1 X-3.8 Y-15 E0.10
G1 X-3.8 Y-20 E0.11
G1 X-3.6 Y-20 E0.12
G1 X-3.6 Y-15 E0.13
G1 X-3.4 Y-15 E0.14
G1 X-3.4 Y-20 E0.15
G1 X-3.2 Y-20 E0.16
G1 X-3.2 Y-15 E0.17
G1 X-3.0 Y-15 E0.18
G1 X-3.0 Y-20 E0.19
G1 X-2.8 Y-20 E0.20
G1 X-2.8 Y-15 E0.21
G1 X-2.6 Y-15 E0.22
G1 X-2.6 Y-20 E0.23
G1 X-2.4 Y-20 E0.24
G1 X-2.4 Y-15 E0.25
G1 X-2.2 Y-15 E0.26
G1 X-2.2 Y-20 E0.27
G1 X-2.0 Y-20 E0.28
G1 X-2.0 Y-15 E0.29
G92 E0
G1 Z1 F360 ; lower bedplate

M107 ; turn off extrusion for extruder 1

;; end of print

G1 F360 ; change speed

M104 S0 ; turn off temperature
G28 X0 ; home X axis
M84      ; disable motors
M140 S0 ; set bed temperature

; end of gcode
```

A.2 All-silver-PDMS G-code script

```

; strain gauge sensor gcode for 1 ink (silver)

; initialisation
G28 ; home all axes
G1 Z5 F ; lift nozzle

; extruder selection
; T0 = extruder 1, T1 = extruder 2
T0

; set up
G21 ; set units to millimeters
G90 ; use absolute coordinates
M82 ; use absolute distances for extrusion
G92 E0

G1 Z0.08 F360 ; layer height
G1 F540 ; print speed 9mm/s

; strain gauge sensing element
; using extruder 1 - graphite ink
G1 X-3.5 Y-16 ; wire 1
G1 X-3.5 Y10 E0.01
G1 X-2.5 Y10 E0.02
G1 X-2.5 Y0 E0.03
G1 X-1.5 Y0 E0.04
G1 X-1.5 Y10 E0.05
G1 X-0.5 Y10 E0.06
G1 X-0.5 Y0 E0.07
G1 X0.5 Y0 E0.08
G1 X0.5 Y10 E0.09
G1 X1.5 Y10 E0.10
G1 X1.5 Y0 E0.11
G1 X2.5 Y0 E0.12
G1 X2.5 Y10 E0.13
G1 X3.5 Y10 E0.14
G1 X3.5 Y-16 E0.15 ; wire 4
G92 E0

; connecting pads and wires 3-4
G1 X3.75 Y-4.5
G1 Z0.080 F360 ; return to layer height
G1 F360
G1 X3.75 Y-4.5 E0.01

```

```
G1 X3.75 Y-5.25 E0.02
G1 X3.25 Y-5.25 E0.03
G1 X3.25 Y-4.5 E0.04
G1 X3.75 Y-4.5 E0.05
G92 E0
G1 X3.5 Y-4.5
G1 X3.5 Y-5 E0.01

; wire 4
G1 X9.5 Y-11 E0.02
G1 X9.5 Y-15 E0.03

; pad 4
G1 X11 Y-15 E0.04
G1 X11 Y-20 E0.05
G1 X8 Y-20 E0.06
G1 X8 Y-15 E0.07
G1 X9.5 Y-15 E0.08
G92 E0
G1 F540
G1 X10.9 Y-15 ; pad infill
G1 X10.9 Y-20 E0.01
G1 X10.8 Y-20 E0.02
G1 X10.8 Y-15 E0.03
G1 X10.7 Y-15 E0.04
G1 X10.7 Y-20 E0.05
G1 X10.6 Y-20 E0.06
G1 X10.6 Y-15 E0.07
G1 X10.5 Y-15 E0.08
G1 X10.5 Y-20 E0.09
G1 X10.4 Y-20 E0.10
G1 X10.4 Y-15 E0.11
G1 X10.3 Y-15 E0.12
G1 X10.3 Y-20 E0.13
G1 X10.2 Y-20 E0.14
G1 X10.2 Y-15 E0.15
G1 X10.1 Y-15 E0.16
G1 X10.1 Y-20 E0.17
G1 X10 Y-20 E0.18
G1 X10 Y-15 E0.19
G1 X9.9 Y-15 E0.20
G1 X9.9 Y-20 E0.21
G1 X9.8 Y-20 E0.22
G1 X9.8 Y-15 E0.23
G1 X9.7 Y-15 E0.24
```

```
G1 X9.7 Y-20 E0.25
G1 X9.6 Y-20 E0.26
G1 X9.6 Y-15 E0.27
G1 X9.5 Y-15 E0.28
G1 X9.5 Y-20 E0.29
G1 X9.4 Y-20 E0.30
G1 X9.4 Y-15 E0.31
G1 X9.3 Y-15 E0.32
G1 X9.3 Y-20 E0.33
G1 X9.2 Y-20 E0.34
G1 X9.2 Y-15 E0.35
G1 X9.1 Y-15 E0.36
G1 X9.1 Y-20 E0.37
G1 X9 Y-20 E0.38
G1 X9 Y-15 E0.39
G1 X8.9 Y-15 E0.40
G1 X8.9 Y-20 E0.41
G1 X8.8 Y-20 E0.42
G1 X8.8 Y-15 E0.43
G1 X8.7 Y-15 E0.44
G1 X8.7 Y-20 E0.45
G1 X8.6 Y-20 E0.46
G1 X8.6 Y-15 E0.47
G1 X8.5 Y-15 E0.48
G1 X8.5 Y-20 E0.49
G1 X8.4 Y-20 E0.50
G1 X8.4 Y-15 E0.51
G1 X8.3 Y-15 E0.52
G1 X8.3 Y-20 E0.53
G1 X8.2 Y-20 E0.54
G1 X8.2 Y-15 E0.55
G1 X8.1 Y-15 E0.56
G1 X8.1 Y-20 E0.57
G92 E0
G1 Z1 F360 ; lower bedplate

; pad 3
G1 X3.5 Y-15
G1 F360
G1 Z0.080 F360 ; return to layer height
G1 X5 Y-15 E0.01
G1 X5 Y-20 E0.02
G1 X2 Y-20 E0.03
G1 X2 Y-15 E0.04
G1 X2 Y-15 E0.05
```

```
G1 X3.5 Y-15 E0.06
G92 E0
G1 F540
G1 X4.9 Y-15 ; pad infill
G1 X4.9 Y-20 E0.01
G1 X4.8 Y-20 E0.02
G1 X4.8 Y-15 E0.03
G1 X4.7 Y-15 E0.04
G1 X4.7 Y-20 E0.05
G1 X4.6 Y-20 E0.06
G1 X4.6 Y-15 E0.07
G1 X4.5 Y-15 E0.08
G1 X4.5 Y-20 E0.09
G1 X4.4 Y-20 E0.10
G1 X4.4 Y-15 E0.11
G1 X4.3 Y-15 E0.12
G1 X4.3 Y-20 E0.13
G1 X4.2 Y-20 E0.14
G1 X4.2 Y-15 E0.15
G1 X4.1 Y-15 E0.16
G1 X4.1 Y-20 E0.17
G1 X4 Y-20 E0.18
G1 X4 Y-15 E0.19
G1 X3.9 Y-15 E0.20
G1 X3.9 Y-20 E0.21
G1 X3.8 Y-20 E0.22
G1 X3.8 Y-15 E0.23
G1 X3.7 Y-15 E0.24
G1 X3.7 Y-20 E0.25
G1 X3.6 Y-20 E0.26
G1 X3.6 Y-15 E0.27
G1 X3.5 Y-15 E0.28
G1 X3.5 Y-20 E0.29
G1 X3.4 Y-20 E0.30
G1 X3.4 Y-15 E0.31
G1 X3.3 Y-15 E0.32
G1 X3.3 Y-20 E0.33
G1 X3.2 Y-20 E0.34
G1 X3.2 Y-15 E0.35
G1 X3.1 Y-15 E0.36
G1 X3.1 Y-20 E0.37
G1 X3 Y-20 E0.38
G1 X3 Y-15 E0.39
G1 X2.9 Y-15 E0.40
G1 X2.9 Y-20 E0.41
```

```

G1 X2.8 Y-20 E0.42
G1 X2.8 Y-15 E0.43
G1 X2.7 Y-15 E0.44
G1 X2.7 Y-20 E0.45
G1 X2.6 Y-20 E0.46
G1 X2.6 Y-15 E0.47
G1 X2.5 Y-15 E0.48
G1 X2.5 Y-20 E0.49
G1 X2.4 Y-20 E0.50
G1 X2.4 Y-15 E0.51
G1 X2.3 Y-15 E0.52
G1 X2.3 Y-20 E0.53
G1 X2.2 Y-20 E0.54
G1 X2.2 Y-15 E0.55
G1 X2.1 Y-15 E0.56
G1 X2.1 Y-20 E0.57
G92 E0
G1 Z1 F360 ; lower bedplate

; connecting pads and wires 1-2
G1 X-3.75 Y-4.5
G1 Z0.080 F360 ; return to layer height
G1 F360
G1 X-3.75 Y-4.5 E0.01
G1 X-3.75 Y-5.25 E0.02
G1 X-3.25 Y-5.25 E0.03
G1 X-3.25 Y-4.5 E0.04
G1 X-3.75 Y-4.5 E0.05
G92 E0
G1 X-3.5 Y-4.5
G1 X-3.5 Y-5 E0.01

; wire 1
G1 X-9.5 Y-11 E0.02
G1 X-9.5 Y-15 E0.03

; pad 1
G1 X-11 Y-15 E0.04
G1 X-11 Y-20 E0.05
G1 X-8 Y-20 E0.06
G1 X-8 Y-15 E0.07
G1 X-9.5 Y-15 E0.08
G92 E0
G1 X-10.9 Y-15 ; pad infill
G1 X-10.9 Y-20 E0.01

```

```
G1 X-10.8 Y-20 E0.02
G1 X-10.8 Y-15 E0.03
G1 X-10.7 Y-15 E0.04
G1 X-10.7 Y-20 E0.05
G1 X-10.6 Y-20 E0.06
G1 X-10.6 Y-15 E0.07
G1 X-10.5 Y-15 E0.08
G1 X-10.5 Y-20 E0.09
G1 X-10.4 Y-20 E0.10
G1 X-10.4 Y-15 E0.11
G1 X-10.3 Y-15 E0.12
G1 X-10.3 Y-20 E0.13
G1 X-10.2 Y-20 E0.14
G1 X-10.2 Y-15 E0.15
G1 X-10.1 Y-15 E0.16
G1 X-10.1 Y-20 E0.17
G1 X-10 Y-20 E0.18
G1 X-10 Y-15 E0.19
G1 X-9.9 Y-15 E0.20
G1 X-9.9 Y-20 E0.21
G1 X-9.8 Y-20 E0.22
G1 X-9.8 Y-15 E0.23
G1 X-9.7 Y-15 E0.24
G1 X-9.7 Y-20 E0.25
G1 X-9.6 Y-20 E0.26
G1 X-9.6 Y-15 E0.27
G1 X-9.5 Y-15 E0.28
G1 X-9.5 Y-20 E0.29
G1 X-9.4 Y-20 E0.30
G1 X-9.4 Y-15 E0.31
G1 X-9.3 Y-15 E0.32
G1 X-9.3 Y-20 E0.33
G1 X-9.2 Y-20 E0.34
G1 X-9.2 Y-15 E0.35
G1 X-9.1 Y-15 E0.36
G1 X-9.1 Y-20 E0.37
G1 X-9 Y-20 E0.38
G1 X-9 Y-15 E0.39
G1 X-8.9 Y-15 E0.40
G1 X-8.9 Y-20 E0.41
G1 X-8.8 Y-20 E0.42
G1 X-8.8 Y-15 E0.43
G1 X-8.7 Y-15 E0.44
G1 X-8.7 Y-20 E0.45
G1 X-8.6 Y-20 E0.46
```

```
G1 X-8.6 Y-15 E0.47
G1 X-8.5 Y-15 E0.48
G1 X-8.5 Y-20 E0.49
G1 X-8.4 Y-20 E0.50
G1 X-8.4 Y-15 E0.51
G1 X-8.3 Y-15 E0.52
G1 X-8.3 Y-20 E0.53
G1 X-8.2 Y-20 E0.54
G1 X-8.2 Y-15 E0.55
G1 X-8.1 Y-15 E0.56
G1 X-8.1 Y-20 E0.57
G92 E0
G1 Z1 F360 ; lower bedplate

; pad 2
G1 X-3.5 Y-15
G1 Z0.080 F360 ; return to layer height
G1 F360
G1 X-5 Y-15 E0.02
G1 X-5 Y-20 E0.03
G1 X-2 Y-20 E0.04
G1 X-2 Y-15 E0.05
G1 X-2 Y-15 E0.06
G1 X-3.5 Y-15 E0.07
G92 E0
G1 F540
G1 X-4.9 Y-15 ; pad infill
G1 X-4.9 Y-20 E0.01
G1 X-4.8 Y-20 E0.02
G1 X-4.8 Y-15 E0.03
G1 X-4.7 Y-15 E0.04
G1 X-4.7 Y-20 E0.05
G1 X-4.6 Y-20 E0.06
G1 X-4.6 Y-15 E0.07
G1 X-4.5 Y-15 E0.08
G1 X-4.5 Y-20 E0.09
G1 X-4.4 Y-20 E0.10
G1 X-4.4 Y-15 E0.11
G1 X-4.3 Y-15 E0.12
G1 X-4.3 Y-20 E0.13
G1 X-4.2 Y-20 E0.14
G1 X-4.2 Y-15 E0.15
G1 X-4.1 Y-15 E0.16
G1 X-4.1 Y-20 E0.17
G1 X-4 Y-20 E0.18
```

```
G1 X-4 Y-15 E0.19
G1 X-3.9 Y-15 E0.20
G1 X-3.9 Y-20 E0.21
G1 X-3.8 Y-20 E0.22
G1 X-3.8 Y-15 E0.23
G1 X-3.7 Y-15 E0.24
G1 X-3.7 Y-20 E0.25
G1 X-3.6 Y-20 E0.26
G1 X-3.6 Y-15 E0.27
G1 X-3.5 Y-15 E0.28
G1 X-3.5 Y-20 E0.29
G1 X-3.4 Y-20 E0.30
G1 X-3.4 Y-15 E0.31
G1 X-3.3 Y-15 E0.32
G1 X-3.3 Y-20 E0.33
G1 X-3.2 Y-20 E0.34
G1 X-3.2 Y-15 E0.35
G1 X-3.1 Y-15 E0.36
G1 X-3.1 Y-20 E0.37
G1 X-3 Y-20 E0.38
G1 X-3 Y-15 E0.39
G1 X-2.9 Y-15 E0.40
G1 X-2.9 Y-20 E0.41
G1 X-2.8 Y-20 E0.42
G1 X-2.8 Y-15 E0.43
G1 X-2.7 Y-15 E0.44
G1 X-2.7 Y-20 E0.45
G1 X-2.6 Y-20 E0.46
G1 X-2.6 Y-15 E0.47
G1 X-2.5 Y-15 E0.48
G1 X-2.5 Y-20 E0.49
G1 X-2.4 Y-20 E0.50
G1 X-2.4 Y-15 E0.51
G1 X-2.3 Y-15 E0.52
G1 X-2.3 Y-20 E0.53
G1 X-2.2 Y-20 E0.54
G1 X-2.2 Y-15 E0.55
G1 X-2.1 Y-15 E0.56
G1 X-2.1 Y-20 E0.57
G92 E0
G1 Z1 F360 ; lower bedplate

M107 ; turn off extrusion for extruder 1

;; end of print
```

```
G1 F360 ; change speed  
M104 S0 ; turn off temperature  
G28 X0 ; home X axis  
M84 ; disable motors  
M140 S0 ; set bed temperature  
;  
; end of gcode
```

A.3 Graphite- & silver-PDMS hybrid G-code script

```
; strain gauge sensor gcode for 2 inks

; initialisation
G28 ; home all axes
G1 Z5 F ; lift nozzle

; extruder selection
; T0 = extruder 1, T1 = extruder 2
T0

; set up
G21 ; set units to millimeters
G90 ; use absolute coordinates
M82 ; use absolute distances for extrusion
G92 E0

G1 Z0.08 F360 ; layer height
G1 F540 ; print speed 9mm/s

; strain gauge sensing element
; using extruder 1 - graphite ink
G1 X-3.5 Y-6 ; start position
G1 X-3.5 Y10 E0.01
G1 X-2.5 Y10 E0.02
G1 X-2.5 Y0 E0.03
G1 X-1.5 Y0 E0.04
G1 X-1.5 Y10 E0.05
G1 X-0.5 Y10 E0.06
G1 X-0.5 Y0 E0.07
G1 X0.5 Y0 E0.08
G1 X0.5 Y10 E0.09
G1 X1.5 Y10 E0.10
G1 X1.5 Y0 E0.11
G1 X2.5 Y0 E0.12
G1 X2.5 Y10 E0.13
G1 X3.5 Y10 E0.14
G1 X3.5 Y-6 E0.15
G92 E0
M107 ; turn off extrusion for extruder 1

;; switch to extruder 2 (T1) with silver ink
T1
G28 ; home extruder 2
```

```

; connecting pads and wires 3-4
G1 X3.75 Y-4.5
G1 Z0.080 F360 ; return to layer height
G1 F360
G1 X3.75 Y-4.5 E0.01
G1 X3.75 Y-5.25 E0.02
G1 X3.25 Y-5.25 E0.03
G1 X3.25 Y-4.5 E0.04
G1 X3.75 Y-4.5 E0.05
G92 E0
G1 X3.5 Y-4.5
G1 X3.5 Y-5 E0.01

; wire 4
G1 X9.5 Y-11 E0.02
G1 X9.5 Y-15 E0.03

; pad 4
G1 X11 Y-15 E0.04
G1 X11 Y-20 E0.05
G1 X8 Y-20 E0.06
G1 X8 Y-15 E0.07
G1 X9.5 Y-15 E0.08
G92 E0
G1 F540
G1 X10.9 Y-15 ; pad infill
G1 X10.9 Y-20 E0.01
G1 X10.8 Y-20 E0.02
G1 X10.8 Y-15 E0.03
G1 X10.7 Y-15 E0.04
G1 X10.7 Y-20 E0.05
G1 X10.6 Y-20 E0.06
G1 X10.6 Y-15 E0.07
G1 X10.5 Y-15 E0.08
G1 X10.5 Y-20 E0.09
G1 X10.4 Y-20 E0.10
G1 X10.4 Y-15 E0.11
G1 X10.3 Y-15 E0.12
G1 X10.3 Y-20 E0.13
G1 X10.2 Y-20 E0.14
G1 X10.2 Y-15 E0.15
G1 X10.1 Y-15 E0.16
G1 X10.1 Y-20 E0.17
G1 X10 Y-20 E0.18
G1 X10 Y-15 E0.19

```

```
G1 X9.9 Y-15 E0.20
G1 X9.9 Y-20 E0.21
G1 X9.8 Y-20 E0.22
G1 X9.8 Y-15 E0.23
G1 X9.7 Y-15 E0.24
G1 X9.7 Y-20 E0.25
G1 X9.6 Y-20 E0.26
G1 X9.6 Y-15 E0.27
G1 X9.5 Y-15 E0.28
G1 X9.5 Y-20 E0.29
G1 X9.4 Y-20 E0.30
G1 X9.4 Y-15 E0.31
G1 X9.3 Y-15 E0.32
G1 X9.3 Y-20 E0.33
G1 X9.2 Y-20 E0.34
G1 X9.2 Y-15 E0.35
G1 X9.1 Y-15 E0.36
G1 X9.1 Y-20 E0.37
G1 X9 Y-20 E0.38
G1 X9 Y-15 E0.39
G1 X8.9 Y-15 E0.40
G1 X8.9 Y-20 E0.41
G1 X8.8 Y-20 E0.42
G1 X8.8 Y-15 E0.43
G1 X8.7 Y-15 E0.44
G1 X8.7 Y-20 E0.45
G1 X8.6 Y-20 E0.46
G1 X8.6 Y-15 E0.47
G1 X8.5 Y-15 E0.48
G1 X8.5 Y-20 E0.49
G1 X8.4 Y-20 E0.50
G1 X8.4 Y-15 E0.51
G1 X8.3 Y-15 E0.52
G1 X8.3 Y-20 E0.53
G1 X8.2 Y-20 E0.54
G1 X8.2 Y-15 E0.55
G1 X8.1 Y-15 E0.56
G1 X8.1 Y-20 E0.57
G92 E0
G1 Z1 F360 ; lower bedplate

; wire 3
G1 X3.5 Y-4
G1 Z0.080 F360 ; return to layer height
G1 F360
```

```
G1 X3.5 Y-15 E0.01

; pad 3
G1 X5 Y-15 E0.02
G1 X5 Y-20 E0.03
G1 X2 Y-20 E0.04
G1 X2 Y-15 E0.05
G1 X2 Y-15 E0.06
G1 X3.5 Y-15 E0.07
G92 E0
G1 F540
G1 X4.9 Y-15 ; pad infill
G1 X4.9 Y-20 E0.01
G1 X4.8 Y-20 E0.02
G1 X4.8 Y-15 E0.03
G1 X4.7 Y-15 E0.04
G1 X4.7 Y-20 E0.05
G1 X4.6 Y-20 E0.06
G1 X4.6 Y-15 E0.07
G1 X4.5 Y-15 E0.08
G1 X4.5 Y-20 E0.09
G1 X4.4 Y-20 E0.10
G1 X4.4 Y-15 E0.11
G1 X4.3 Y-15 E0.12
G1 X4.3 Y-20 E0.13
G1 X4.2 Y-20 E0.14
G1 X4.2 Y-15 E0.15
G1 X4.1 Y-15 E0.16
G1 X4.1 Y-20 E0.17
G1 X4 Y-20 E0.18
G1 X4 Y-15 E0.19
G1 X3.9 Y-15 E0.20
G1 X3.9 Y-20 E0.21
G1 X3.8 Y-20 E0.22
G1 X3.8 Y-15 E0.23
G1 X3.7 Y-15 E0.24
G1 X3.7 Y-20 E0.25
G1 X3.6 Y-20 E0.26
G1 X3.6 Y-15 E0.27
G1 X3.5 Y-15 E0.28
G1 X3.5 Y-20 E0.29
G1 X3.4 Y-20 E0.30
G1 X3.4 Y-15 E0.31
G1 X3.3 Y-15 E0.32
G1 X3.3 Y-20 E0.33
```

```
G1 X3.2 Y-20 E0.34
G1 X3.2 Y-15 E0.35
G1 X3.1 Y-15 E0.36
G1 X3.1 Y-20 E0.37
G1 X3 Y-20 E0.38
G1 X3 Y-15 E0.39
G1 X2.9 Y-15 E0.40
G1 X2.9 Y-20 E0.41
G1 X2.8 Y-20 E0.42
G1 X2.8 Y-15 E0.43
G1 X2.7 Y-15 E0.44
G1 X2.7 Y-20 E0.45
G1 X2.6 Y-20 E0.46
G1 X2.6 Y-15 E0.47
G1 X2.5 Y-15 E0.48
G1 X2.5 Y-20 E0.49
G1 X2.4 Y-20 E0.50
G1 X2.4 Y-15 E0.51
G1 X2.3 Y-15 E0.52
G1 X2.3 Y-20 E0.53
G1 X2.2 Y-20 E0.54
G1 X2.2 Y-15 E0.55
G1 X2.1 Y-15 E0.56
G1 X2.1 Y-20 E0.57
G92 E0
G1 Z1 F360 ; lower bedplate

; connecting pads and wires 1-2
G1 X-3.75 Y-4.5
G1 Z0.080 F360 ; return to layer height
G1 F360
G1 X-3.75 Y-4.5 E0.01
G1 X-3.75 Y-5.25 E0.02
G1 X-3.25 Y-5.25 E0.03
G1 X-3.25 Y-4.5 E0.04
G1 X-3.75 Y-4.5 E0.05
G92 E0
G1 X-3.5 Y-4.5
G1 X-3.5 Y-5 E0.01

; wire 1
G1 X-9.5 Y-11 E0.02
G1 X-9.5 Y-15 E0.03

; pad 1
```

```
G1 X-11 Y-15 E0.04
G1 X-11 Y-20 E0.05
G1 X-8 Y-20 E0.06
G1 X-8 Y-15 E0.07
G1 X-9.5 Y-15 E0.08
G92 E0
G1 F540
G1 X-10.9 Y-15 ; pad infill
G1 X-10.9 Y-20 E0.01
G1 X-10.8 Y-20 E0.02
G1 X-10.8 Y-15 E0.03
G1 X-10.7 Y-15 E0.04
G1 X-10.7 Y-20 E0.05
G1 X-10.6 Y-20 E0.06
G1 X-10.6 Y-15 E0.07
G1 X-10.5 Y-15 E0.08
G1 X-10.5 Y-20 E0.09
G1 X-10.4 Y-20 E0.10
G1 X-10.4 Y-15 E0.11
G1 X-10.3 Y-15 E0.12
G1 X-10.3 Y-20 E0.13
G1 X-10.2 Y-20 E0.14
G1 X-10.2 Y-15 E0.15
G1 X-10.1 Y-15 E0.16
G1 X-10.1 Y-20 E0.17
G1 X-10 Y-20 E0.18
G1 X-10 Y-15 E0.19
G1 X-9.9 Y-15 E0.20
G1 X-9.9 Y-20 E0.21
G1 X-9.8 Y-20 E0.22
G1 X-9.8 Y-15 E0.23
G1 X-9.7 Y-15 E0.24
G1 X-9.7 Y-20 E0.25
G1 X-9.6 Y-20 E0.26
G1 X-9.6 Y-15 E0.27
G1 X-9.5 Y-15 E0.28
G1 X-9.5 Y-20 E0.29
G1 X-9.4 Y-20 E0.30
G1 X-9.4 Y-15 E0.31
G1 X-9.3 Y-15 E0.32
G1 X-9.3 Y-20 E0.33
G1 X-9.2 Y-20 E0.34
G1 X-9.2 Y-15 E0.35
G1 X-9.1 Y-15 E0.36
G1 X-9.1 Y-20 E0.37
```

```

G1 X-9 Y-20 E0.38
G1 X-9 Y-15 E0.39
G1 X-8.9 Y-15 E0.40
G1 X-8.9 Y-20 E0.41
G1 X-8.8 Y-20 E0.42
G1 X-8.8 Y-15 E0.43
G1 X-8.7 Y-15 E0.44
G1 X-8.7 Y-20 E0.45
G1 X-8.6 Y-20 E0.46
G1 X-8.6 Y-15 E0.47
G1 X-8.5 Y-15 E0.48
G1 X-8.5 Y-20 E0.49
G1 X-8.4 Y-20 E0.50
G1 X-8.4 Y-15 E0.51
G1 X-8.3 Y-15 E0.52
G1 X-8.3 Y-20 E0.53
G1 X-8.2 Y-20 E0.54
G1 X-8.2 Y-15 E0.55
G1 X-8.1 Y-15 E0.56
G1 X-8.1 Y-20 E0.57
G92 E0
G1 Z1 F360 ; lower bedplate

;wire 2
G1 X-3.5 Y-4
G1 Z0.080 F360 ; return to layer height
G1 F360
G1 X-3.5 Y-15 E0.01

; pad 2
G1 X-5 Y-15 E0.02
G1 X-5 Y-20 E0.03
G1 X-2 Y-20 E0.04
G1 X-2 Y-15 E0.05
G1 X-2 Y-15 E0.06
G1 X-3.5 Y-15 E0.07
G92 E0
G1 F540
G1 X-4.9 Y-15 ; pad infill
G1 X-4.9 Y-20 E0.01
G1 X-4.8 Y-20 E0.02
G1 X-4.8 Y-15 E0.03
G1 X-4.7 Y-15 E0.04
G1 X-4.7 Y-20 E0.05
G1 X-4.6 Y-20 E0.06

```

```
G1 X-4.6 Y-15 E0.07
G1 X-4.5 Y-15 E0.08
G1 X-4.5 Y-20 E0.09
G1 X-4.4 Y-20 E0.10
G1 X-4.4 Y-15 E0.11
G1 X-4.3 Y-15 E0.12
G1 X-4.3 Y-20 E0.13
G1 X-4.2 Y-20 E0.14
G1 X-4.2 Y-15 E0.15
G1 X-4.1 Y-15 E0.16
G1 X-4.1 Y-20 E0.17
G1 X-4 Y-20 E0.18
G1 X-4 Y-15 E0.19
G1 X-3.9 Y-15 E0.20
G1 X-3.9 Y-20 E0.21
G1 X-3.8 Y-20 E0.22
G1 X-3.8 Y-15 E0.23
G1 X-3.7 Y-15 E0.24
G1 X-3.7 Y-20 E0.25
G1 X-3.6 Y-20 E0.26
G1 X-3.6 Y-15 E0.27
G1 X-3.5 Y-15 E0.28
G1 X-3.5 Y-20 E0.29
G1 X-3.4 Y-20 E0.30
G1 X-3.4 Y-15 E0.31
G1 X-3.3 Y-15 E0.32
G1 X-3.3 Y-20 E0.33
G1 X-3.2 Y-20 E0.34
G1 X-3.2 Y-15 E0.35
G1 X-3.1 Y-15 E0.36
G1 X-3.1 Y-20 E0.37
G1 X-3 Y-20 E0.38
G1 X-3 Y-15 E0.39
G1 X-2.9 Y-15 E0.40
G1 X-2.9 Y-20 E0.41
G1 X-2.8 Y-20 E0.42
G1 X-2.8 Y-15 E0.43
G1 X-2.7 Y-15 E0.44
G1 X-2.7 Y-20 E0.45
G1 X-2.6 Y-20 E0.46
G1 X-2.6 Y-15 E0.47
G1 X-2.5 Y-15 E0.48
G1 X-2.5 Y-20 E0.49
G1 X-2.4 Y-20 E0.50
G1 X-2.4 Y-15 E0.51
```

```
G1 X-2.3 Y-15 E0.52
G1 X-2.3 Y-20 E0.53
G1 X-2.2 Y-20 E0.54
G1 X-2.2 Y-15 E0.55
G1 X-2.1 Y-15 E0.56
G1 X-2.1 Y-20 E0.57
G92 E0
G1 Z1 F360 ; lower bedplate

M107 ; turn off extrusion for extruder 1

;; end of print

G1 F360 ; change speed

M104 S0 ; turn off temperature
G28 X0 ; home X axis
M84 ; disable motors
M140 S0 ; set bed temperature

; end of gcode
```